UNIVERSITY OF OKLAHOMA

GRADUATE COLLEGE

CASE STUDY: INTEGRATED CORE MODELING AND SIMULATION OF UNCONVENTIONAL HYDRAULICALLY FRACTURED WELLS IN THE DELAWARE BASIN

A THESIS

SUBMITTED TO THE GRADUATE FACULTY

in partial fulfillment of the requirements for the

Degree of

MASTER OF SCIENCE

By

WILLIAM ROY HEFNER
Norman, Oklahoma
2020

CASE STUDY: INTEGRATED CORE MODELING AND SIMULATION OF UNCONVENTIONAL HYDRAULICALLY FRACTURED WELLS IN THE DELAWARE BASIN

A THESIS APPROVED FOR THE
MEWBOURNE SCHOOL OF PETROLEUM AND GEOLOGICAL ENGINEERING

BY THE COMMITTEE CONSISTING OF

Dr. Rouzbeh Ghanbarnezhad Moghanloo, Chair

Dr. Deepak Devegowda

Dr. Catalin Teodoriu

To my wife, Liz, and team for their unconditional support throughout my professional career: I could not have done this without you.

Acknowledgements

I highly express my appreciation to my advisor, Dr. Rouzbeh Moghanloo, for his guidance, dedication, motivational aid, and general life advice through this work and challenges with my graduate studies at the University of Oklahoma. This thesis would not have been possible without his critical acumen and valuable insights into reservoir engineering principles.

I also extend my appreciation to Dr. Deepak Devegowda and Dr. Catalin Teodoriu for serving on my committee, providing expertise in their technical coursework, and contributing to the university in many unique ways. Without the many courses I participated in with these professors, I do not believe pursuing a master's degree would have been worth my time.

Additionally, I would like to express my gratitude to those who aided this work and collaborated on multiple other works. Thanks to Davud Davudov, Richard Brito, Dr. Roger Slatt, Tien Phan, Any Ordonez, and all Mewbourne professors for their assistance along the way. Also, thanks to SLB Technical Support for the constant aid from beginning to end.

Table of Contents

Acknowledgments…….. iv

List of Tables…… viii

List of Figures……ix

Abstract……..xii

Chapter 1: Introduction

1.1 Study Location and Well Information…….. 3

1.2 Objectives…… 4

1.3 Outline……...4

Chapter 2: Geological Setting and Core Analysis……. 6

2.1 Introduction to the Delaware Basin……. 6

2.2 Core Analysis…….10

2.2.1 Depositional Facies……10

2.2.2 Minerology…….13

2.2.3 Petrophysical Properties…….17

2.2.4 Geomechanical Properties……. 20

2.2.5 Natural Fractures……22

Chapter 3: Reservoir Characterization and Geological Modeling……...23

3.1 Structural and Stratigraphic Modeling……...23

3.2 Petrophysical Properties Modeling……... …….25

3.2.1 Porosity and Permeability…….. 25

3.2.2 Water Saturation and Net-to-Gross……... 27

3.3 Mechanical Properties Modeling…….. 28

Chapter 4: Hydraulic Fracture Model…….. 32

4.1 HFM Grid Properties Modeling…… 32

4.2 Hydraulic Fracture Treatment Design and Pumping Schedule…….35

4.3 Hydraulic Fracturing Simulation Results……..37

Chapter 5: Reservoir Simulation……...41

5.1 Simulation Model……41

5.2 Compositional Fluid Model and Relative Permeability……..42

5.3 Base Case Simulation Results and Sensitivity Analysis…….46

Chapter 6: Miscible Gas Injection Simulation……..47

6.1 MMP Determination……... 50

6.2 Well Schedule Design……50

6.3 Sensitivity Analysis…….56

Chapter 7: Discussion and Limitations……61

Chapter 8: Conclusions……64

Nomenclature……66

References……..67

List of Tables

Table 1. Petrophysical property data analysis types performed on whole core of pilot well…… 18

Table 2. Additional core testing analysis types for whole core in pilot well…….21

Table 3. Observed pumping schedule for development well for 22 stages of design……... 36

Table 4. Average hydraulic fracture geometries for each zone in the wellbore simulation…….. 39

Table 5. Reservoir initial input data for simulation from field estimates…….. 42

Table 6. Recombination of components from separator values in Winprop……. 43

Table 7. Relative permeability endpoints and Corey exponents from Ojha et al., 2017……... 45

Table 8. Outcome of 16 cases for injection rate for each type of stream and the associated incremental recovery……..57

Table 9. Time to injection outcomes for each stream type with incremental recovery results for 16 cases…….. 60

List of Figures

Figure 1. Case study workflow for the design of the 3D model of the Wolfcamp A-XY……...2

Figure 2. Development well location shown by the red star in the Delaware Basin……..3

Figure 3. Stratigraphic column of Delaware Basin along with Wolfcamp zones……8

Figure 4. Map of Delaware Basin showing relative location of development area……9

Figure 5. L1 facies (most dominant) and L2 facies (less dominant) of Wolfcamp A core……... 11

Figure 6. L1 facies (most dominant) depicting fine-grained carbonates and siltstones…….11

Figure 7. L2 facies (less dominant) depicting coarser-grained siltstone to carbonate grains…… 12

Figure 8. Transition from TBSG to Wolfcamp A in whole core from pilot well…….. 12

Figure 9. Mineral volumes by percent in whole core for pilot well…….. 14

Figure 10. Synthetic gamma ray log determined from empirical equation of potassium, thorium and uranium……... 15

Figure 11. Synthetic total gamma ray log compared to mineral components of the whole core in pilot well…… 16

Figure 12. Permeability-porosity cross-plot of whole core in pilot well. Transform equation used as a potential derivation during petrophysical modeling……... 18

Figure 13. Water saturation and porosity cross-plot from Dean-Stark technique performed on pilot well…… 19

Figure 14. MICP data determining capillary pressure and confirming saturations of whole core in pilot well…… 20

Figure 15. Logs created from core data mechanical properties in pilot well…….21

Figure 16. Well log depiction showing gamma ray, bulk density, porosity, mineral volumes, and the well tops for the Wolfcamp A-XY pilot well…….. 24
Figure 17. Facies model depicted in 3D for Wolfcamp A-XY focus interval……...25
Figure 18. Porosity (A) and Permeability (B) depiction of Wolfcamp A-XY area using core data, well log calculations, and a porosity-permeability transform……27
Figure 19. Water Saturation (C) and Net-to-Gross (D) depiction of Wolfcamp A-XY area using core data, well logs, and the Dual Water model…… 28
Figure 20. Young's Modulus and Poisson's Ratio logs of Wolfcamp A-XY area using core data, sonic well logs, and the geomechanical calculations…….30
Figure 21. Poisson's Ratio (E) and Young's Modulus (F) depiction of Wolfcamp A-XY area using core data, sonic well logs, and the geomechanical calculations……...31
Figure 22. Total stress distribution along the wellbore in a depiction from the hydraulic fracturing model in GOHFER……34
Figure 23. Graphical depiction of pumping schedule for 1 stage of the 22 stages…… 37
Figure 24. Treatment pressure match for one stage of hydraulic fracture design……..38
Figure 25. Point data imported as attributes into the 3D geological grid…….. 40
Figure 26. Upscaled depiction of point data into petrophysical transmissibility properties……..40
Figure 27. Phase envelope for the resulting compositional fluid model……44
Figure 28. Relative permeability estimates recreated from Ojha et al., 2017……45
Figure 29. (A) Base Case oil production rate over 17 years. (B) Base Case gas production rate over 17 years……..46
Figure 30. Compositional production rate during the 17-year Base Case……47

Figure 31. Tornado plot for sensitivity analysis of input parameters for 3D model……..48

Figure 32. Illustration of cyclic injection strategy for EOR miscible gas injection…….. 50

Figure 33. Production profile of HC gas during the primary and post injection phases……....51

Figure 34. Average reservoir pressure during HC gas injection strategy…….. 52

Figure 35. Distribution of HC gas injected into the formation and fractures…… 52

Figure 36. C7+ production tracking during HC gas injection strategy……..53

Figure 37. CO_2 injection production profile for 3 cycles of injection……... 54

Figure 38. C7+ compositional production tracking for CO_2 injection strategy. Average reservoir pressure is also graphically shown…….55

Figure 39. CO_2 distribution after injection in the 3D model……. 55

Figure 40. (A) Cumulative oil and rate comparison between HC gas, CO_2, and Base Case. (B) C7+ compositional production tracking for the 3 different cases……..57

Figure 41. HC gas C7+ mole fraction remaining after 17 years……58

Figure 42. CO_2 injection C7+ mole fraction remaining after 17 years……. 58

Figure 43. Time to injection production rate comparison between CO_2 injection and HC gas injection……..59

Figure 44. Time to injection cumulative production comparison between CO_2 injection and HC gas injection……... 60

Abstract

The Early Paleozoic Wolfcamp formation is one of the main unconventional reservoirs in the Delaware Basin, and highly targeted by U.S. companies. Innovative completion techniques and representative core analysis have become more prevalent, while undeveloped location numbers are decreasing. Despite the increase in information gathering, integration of data for the lifecycle of the well is challenging prior to development. The scope of this study is to integrate geological, compositional fluid, and hydraulic fracturing data obtained from the field into a reliable 3D model to evaluate reservoir and production performance of the lifecycle a multi-stage hydraulically fractured well in the Wolfcamp A-XY formation of the Delaware Basin.

This case study illustrates the necessity of reservoir model implementation into the development process. A 3D geological and geomechanical reservoir model was constructed based on core and well log data obtained from a vertical pilot location in Eddy County, NM. The geomechanical model output was implemented into a hydraulic fracture simulator, consisting of 22 stages for an over 4000-foot horizontal development well, to evaluate and produce key fracture geometries and properties used in the simulation model. A compositional fluid simulator was then used to build an 11-component compositional fluid model representative of produced samples from the initial production of a development well. Then, two EOR miscible gas injection strategies, hydrocarbon gas and CO_2, were used within the compositional model to examine the effect of injection rate, time to injection, and type of gas injected on the recovery of hydrocarbons. The results of the reservoir modeling show uncertainty greatly reduced when employing core data prior to simulation. Simulation results indicate that both hydrocarbon gas and CO_2 miscible injection strategies yields incremental recoveries of 2 to 9.5%. Additionally, resulting analysis of

sensitivities on production performance reveals that injection rate and time to injection are dependent on the type of gas injected. Results for each simulation illustrate the potential for enhanced recovery during the life of the well.

Chapter 1: Introduction

For about a century the Permian Basin has produced over 34 billion barrels of oil and over 110 trillion cubic feet of natural gas, as of December 2019. Horizontal drilling, extended laterals, hydraulic fracturing, and core analysis implementation have advanced during the most recent decade and reversed the production decline in the basin, which has pushed the boundaries of its production, specifically with unconventional targets, and surpassed its peak from the 1970s (EIA, 2020). During 2019, over 37% of total U.S. oil production and 10% of the total gas production was accounted for in the Permian Basin. The EIA estimates its remaining proven reserves to be over 80 billion barrels of oil and 500 trillion cubic feet of gas, making it the most prolific basins in the U.S. (EIA, 2019).

The Delaware Basin, the western portion of the Permian Basin, has seen a large increase in drilling and development activity in recent years. This has happened with innovation in the fields of extended lateral application, hydraulic fracturing technology, and core analysis that aids in the production from unconventional formations. In fact, estimates of total reserves for the Delaware Basin include over 46 billion barrels of oil and 280 trillion cubic feet of natural gas in just the Bone Spring and Wolfcamp formations (EIA, 2020).

Even with technological advancements of unconventional development in the Delaware Basin, unconventional well production declines significantly over the lifetime of the well, which leads to low recovery factors. One type of process to increase the recovery factor is that of Enhanced Oil Recovery (EOR). These techniques have yielded an increase of 2-10 billion barrels of oil equivalent with just a small increase in recovery factor (Hawthorne, 2013). The most typical process used in EOR is that of miscible gas injection. Due to the large infrastructure and natural

gas production in the Delaware Basin, miscible natural gas and CO_2 injection have become the most feasible techniques. Currently, multiple miscible gas injection EOR pilot projects are underway in the Permian Basin (EIA, 2019).

This thesis attempts to integrate high quality well-log, core, fluid composition, pressure, and a multitude of additional data to develop a geologic, hydraulic fracture, and reservoir simulation model for the life cycle of a development well from the onset production to enhanced oil recovery (EOR) processes. The formation that is the focus of this study is the Wolfcamp A-XY. The study workflow is illustrated in Figure 1.

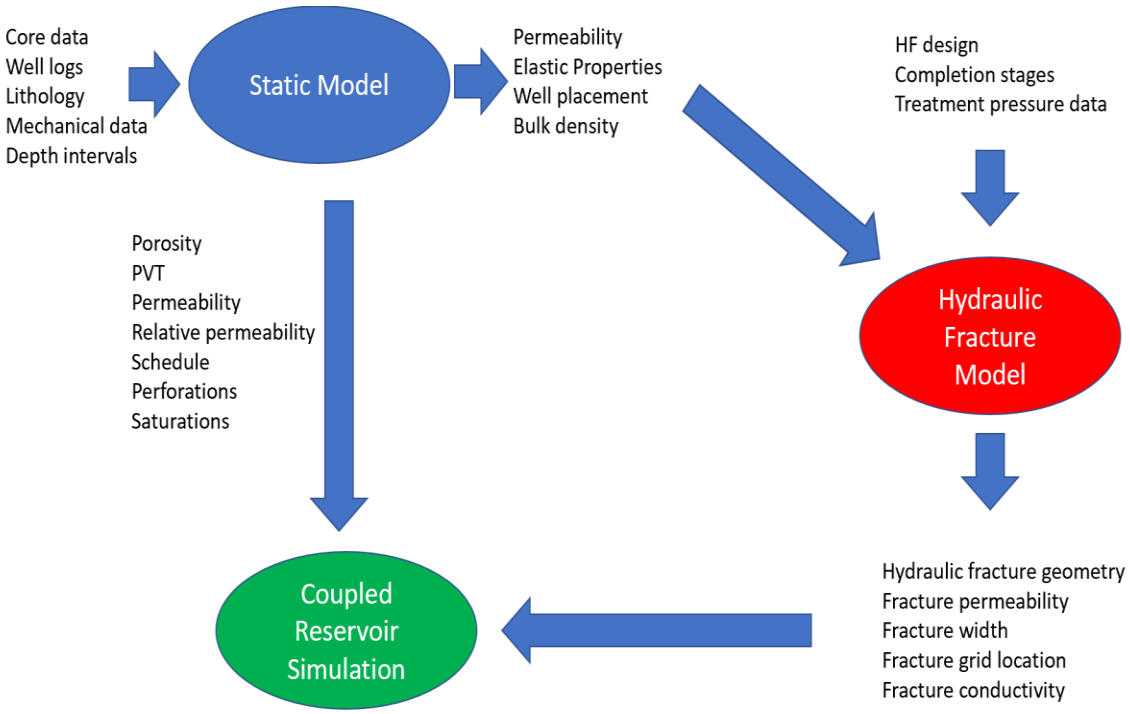

Figure 1. Case study workflow for the design of the 3D model of the Wolfcamp A-XY.

1.1 Study Location and Well Information

This study is located in the Northern Delaware Basin, denoted by the red star, near the basin's Northwestern Shelf. Most data used in this study was provided by an undisclosed oil and gas company. Due to the location being in an active development area with a high amount of drilling, precise locations are not provided.

The well being used in this study is a development well in the Wolfcamp A-XY formation for a development area. The coupling of geology and production are not well known for this target. This is the only well in the vicinity of its kind with a modern completion. It will be used as a baseline for future wells in the entire region to study.

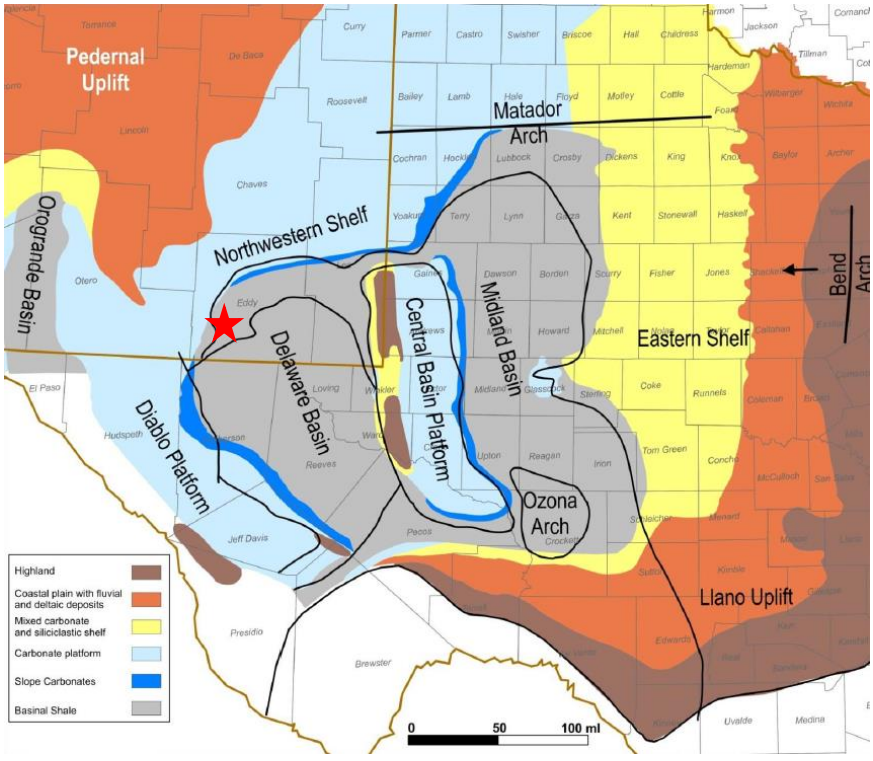

Figure 2. Development well location shown by the red star in the Delaware Basin (Kvale et al., 2016)

1.2 Objectives

The main objectives of this study are, as follows:

- Construct reliable 3D geological, geomechanical, and hydraulic fracturing models by integrating core and well-log data to depict the variability in the petrophysics and stratigraphic features of the Wolfcamp A-XY.
- Implement the resulting attributes and parameters from the 3D models into a numerical reservoir simulation to understand the lifecycle of a development well.
- Gain valuable understanding of the EOR miscible gas injection process and the effect it has on well production performance.

1.4 Outline

This study is organized as follows.

Chapter 2 focuses on the geological environment and core analysis implemented for a pilot well in the Wolfcamp A-XY formation. The output of the core analysis aided in determining the depositional facies, minerology, petrophysical attributes, and geomechanical properties implemented into the 3D model.

Chapter 3 introduces and presents the methodology to build 3D earth model and geomechanical model. Core data from Chapter 2 and well log data analysis are implemented in this section of the study.

Chapter 4 describes the data and workflow used to determine the hydraulic fracture properties and design imported into the 3D model. This model is based on the geomechanical

earth model in Chapter 3 implemented into the hydraulic fracturing simulator prior to use. A treatment history match from field data is summarized in the chapter, as well.

Chapter 5 presents the integrated simulation scenario for the base case model during the first 17 years of the well's life. Properties from the 3D models, fluid model, hydraulic fracture model, and natural fracture data are implemented in this step of the study.

Chapter 6 presents EOR miscible gas injection techniques during the later parts of the wells lifecycle. This chapter presents two methods, hydrocarbon gas (HC Gas) and CO_2, for cycling recovery. The huff-n-puff schedule is the primary focus. This chapter also illustrates a sensitivity effect in timing of EOR implementation and type of gas injected.

Chapter 2: Geological Setting and Core Analysis

This chapter focuses on the analysis of real-time data prior to implementing each piece into the 3D reservoir model of the Wolfcamp A-XY formation. The analysis is focused on whole core, rotary side wall core, and well-log measurements.

2.1 Introduction to the Delaware Basin

The Delaware Basin is part of a stable, shallow, ancestral Permian Basin referred to as the Tobosa Basin. Early Paleozoic deposition was dominated by shelf and ramp carbonates until a ring of uplifts encircled the basin in Mississippian time. Early Mississippian carbonate deposits gave way to terrigenous mud deposition which continued through Early Pennsylvanian time. In the Late Mississippian, a fault bounded horst began to rise in the center of the basin. Known as the Central Basin Platform, this North-South trending, positive structural element subdivided the Tobosa Basin in the Midland and Delaware Basins (Figure 2). An East-West trending fault zone, related to the evolution of the Central Basin Platform, divides the basin into Northern and Southern portions. The Delaware Basin was structurally deep by Late Pennsylvanian and remained so through Permian time. Following the cessation of movement in Lower Permian time, massive carbonate reefs built out from the submarine fault scarps, separating the shelf from the deep water basin. Consequently, evaporate and carbonates were deposited on the Northwestern Shelf and Central Basin Platform; whereas, deep water siliciclastics filled the central basin. This facies division prevailed during the Late Wolfcampian, Leonardian, and Guadalupian. Late Permian marine regression led to the deposition of seal evaporates. Although tectonic activity was mild, the basin continued to subside. Permian strata are overlain by some 2000 feet of continental and

shallow marine Triassic and Cretaceous deposits. Tertiary tectonism uplifted the western edge of the basin, resulting in a gentle, eastward tilt (Rittenhouse et al., 2017).

Wolfcamp Shale, a mixture of shale, carbonate, and sandstone, was deposited during the Wolfcampian Age and is present in the entirety of the Permian Basin, while being prolific in the Delaware Basin. It comfortably overlies the Virgil-aged Cisco formation, part of the Pennsylvanian Era (Figure 3). The formation is a highly heterogeneous unit, comprised mostly of organic-rich shale and carbonate bedding near the outer edges of the basin. Lithology, thickness, and depth of each interval show high variability across the entire basin. The Wolfcamp thickness varies between 800 and 7000 feet across the Delaware Basin (EIA, 2019). The Wolfcamp is subdivided into four stacked benches, the A, B, C, and D, with the A and B being the most prolific hydrocarbon producing zones. Porosity ranges from 2-12%, while permeability can be as low as 10 millidarcies, requiring the need for hydraulic fracturing operations to access hydrocarbons. For the purposes of this study, a focus was on the Wolfcamp A-XY, with the location in Eddy County, NM (Figure 4).

In the Delaware Basin, more subdivision of the Wolfcamp A has been shown to be present. It can be divided between 5 distinct zones, or benches, that are comprised of shaly-sandstone, interbedded with carbonate elements. The cross-section below illustrates each of these benches, starting with the Wolfcamp A and ending with the Wolfcamp Y.

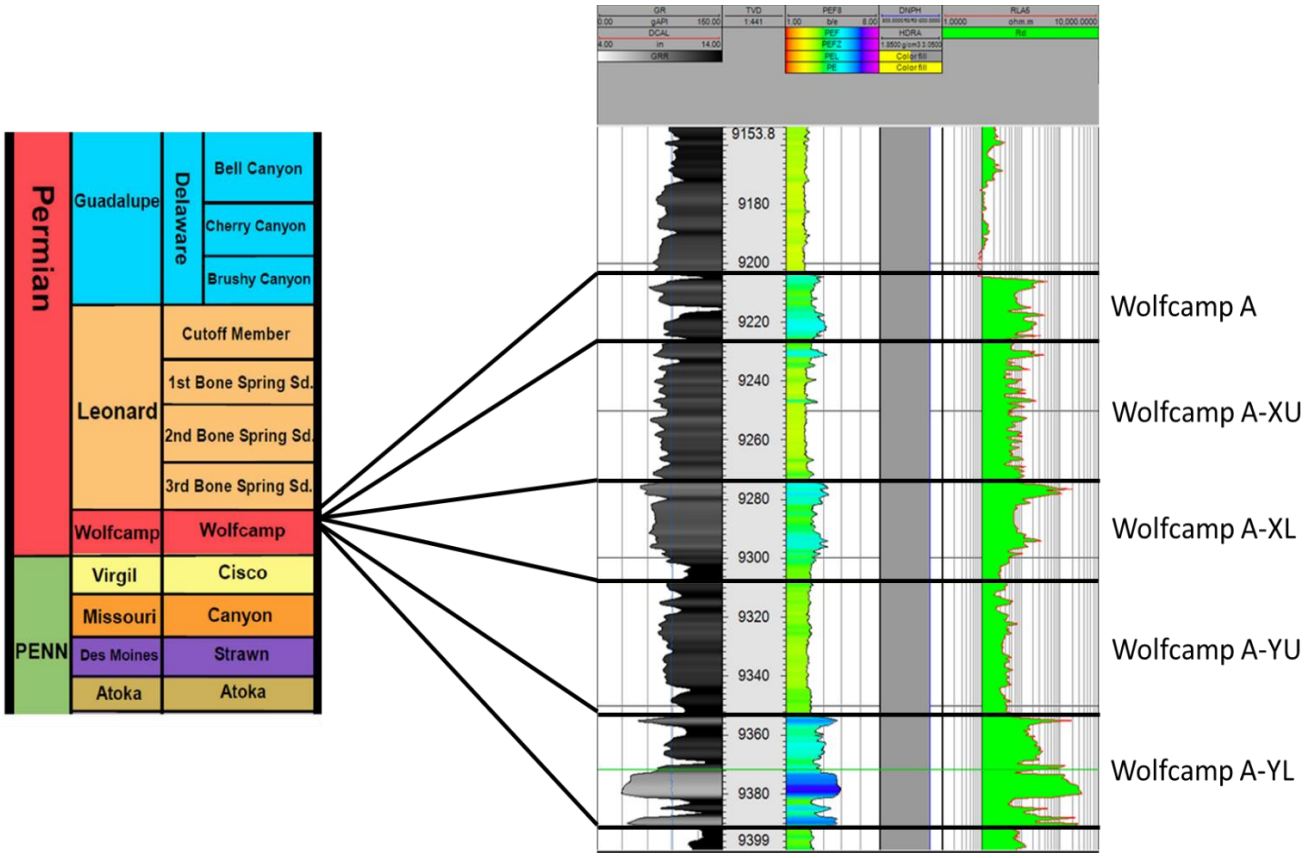

Figure 3. Stratigraphic column of Delaware Basin along with Wolfcamp zones broken out, with current field log. (Kvale et al., 2016)

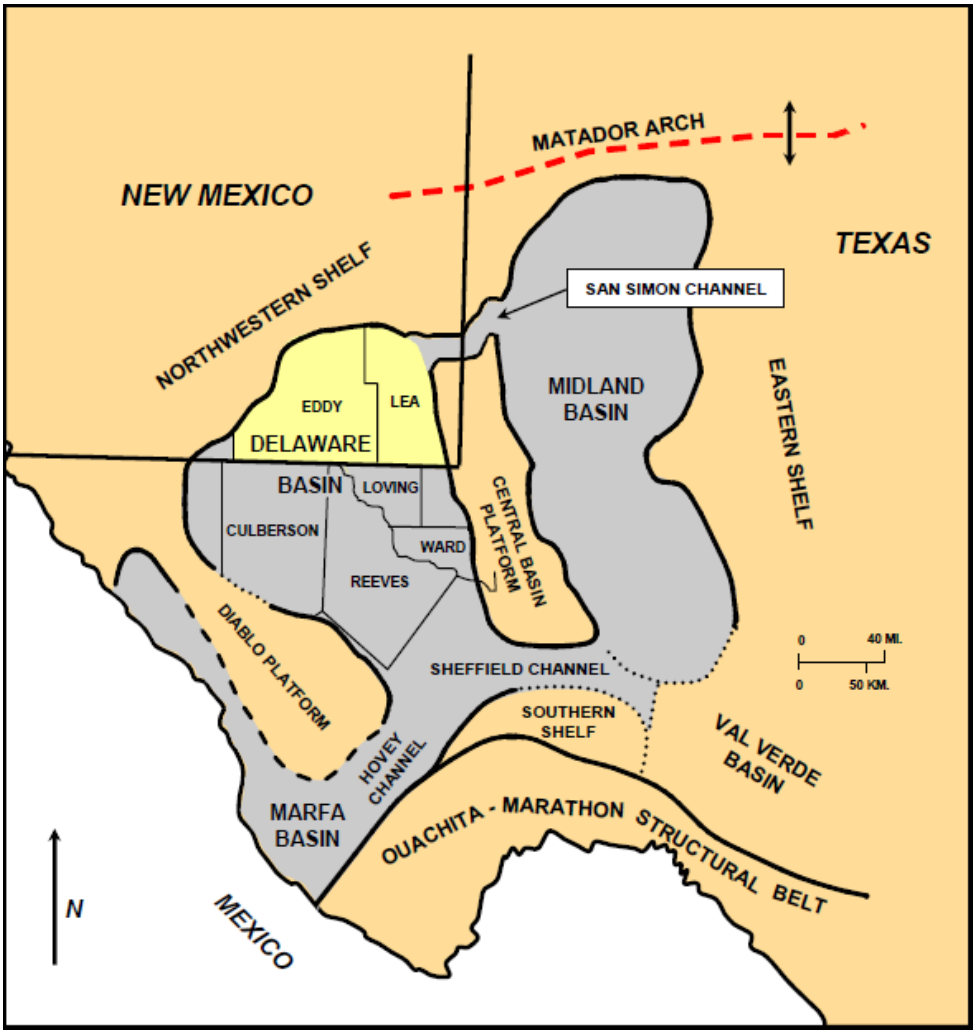

Figure 4. Map of Delaware Basin showing relative location of development area in yellow (Cullick et al., 2014)

2.2 Core Analysis

Obtaining quality core data is an important element to upscaling from core depositional facies into a geologic reservoir model. The data analysis consisted of approximately 6,000 feet of whole core, using a suite of analysis types, including: XRD, permeability, porosity, capillary pressure, and multiple other analysis. The well used to acquire the whole core contributing to this study is the pilot well for an undisclosed development area in Eddy County, NM.

2.2.1 Depositional Facies

The depositional setting of all the lithofacies described in this core is on the deep water slope or in the deeper water setting of the Delaware Basin. The Paleozoic deeper water basins were "starved basins." Very little biota lived in the open-sea water column. Most of the sediment was transported in from the shallower shelf by gravity-flow deposition or by hemipelagic plumes from the shelf. Also, large amount of dust is thought to have been deposited into the basin by eolian processes followed by suspension deposition by marine snow. After sediments were deposited, some were reworked by bottom currents (Driskill et al., 2018). The laminations seen in thin sections may have formed by bottom-currents or suspension processes. Many of the thin sections show diffused to distinct burrows. Soft-sediment deformation was observed in a few thin sections, which suggest slumping. The core described throughout the process is focused mainly on the Wolfcamp A-XY.

The Wolfcamp A-XY formation is comprised of 3 different rock types. The reservoir dominant facies is composed of a fine-grained carbonates and siltstones/mudstones. Nodules, typically made up of replaced radiolarians, are present in this interval (Figure 6). The silica-rich mudstone aids in the brittleness of the rock, preserving most of its porosity. This facies is

interbedded with organic-rich mudstones that is part of the reservoir package that is currently being produced. The second most prolific facies is more calcareous, and varies from calcite cemented coarse grained-siltstone to carbonate grains (Figure 7). A transition into the Wolfcamp A is shown in the pilot well whole core in Figure 8. The facies compositions are listed in the following pie charts as L1 (most dominant) through L2 (least dominant) (Figure 5).

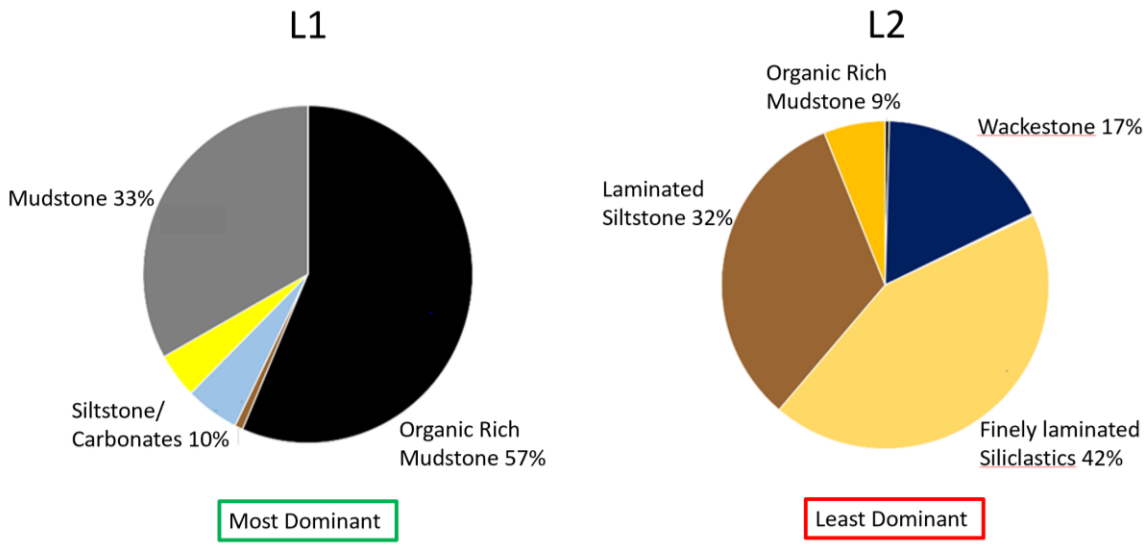

Figure 5. L1 facies (most dominant) and L2 facies (less dominant) of Wolfcamp A core.

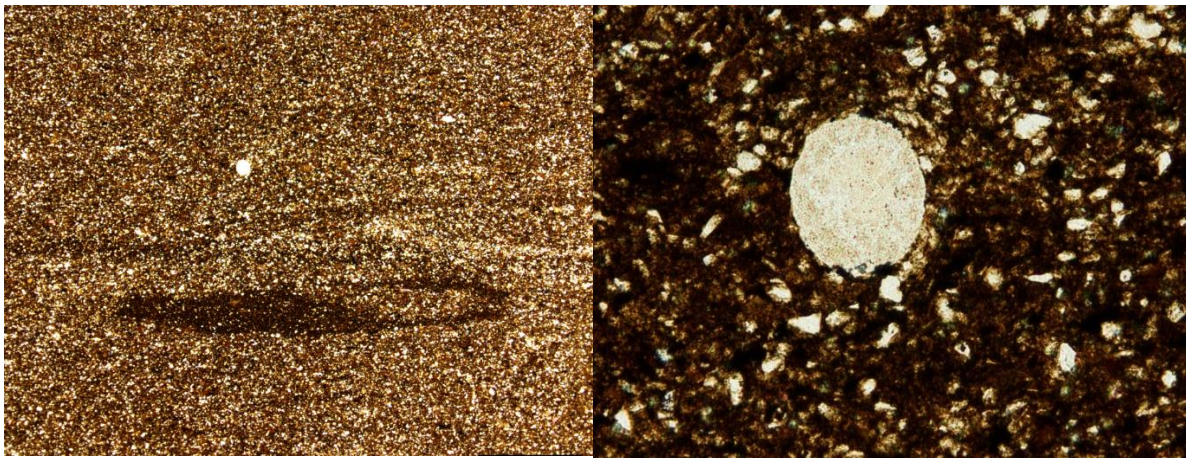

Figure 6. L1 facies (most dominant) depicting fine-grained carbonates and siltstones/mudstones.

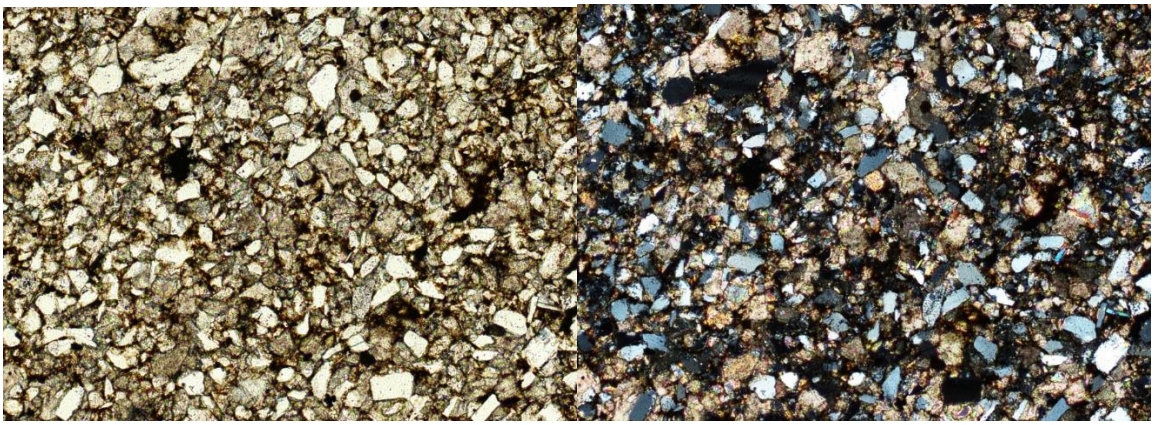

Figure 7. L2 facies (less dominant) depicting coarser-grained siltstone to carbonate grains.

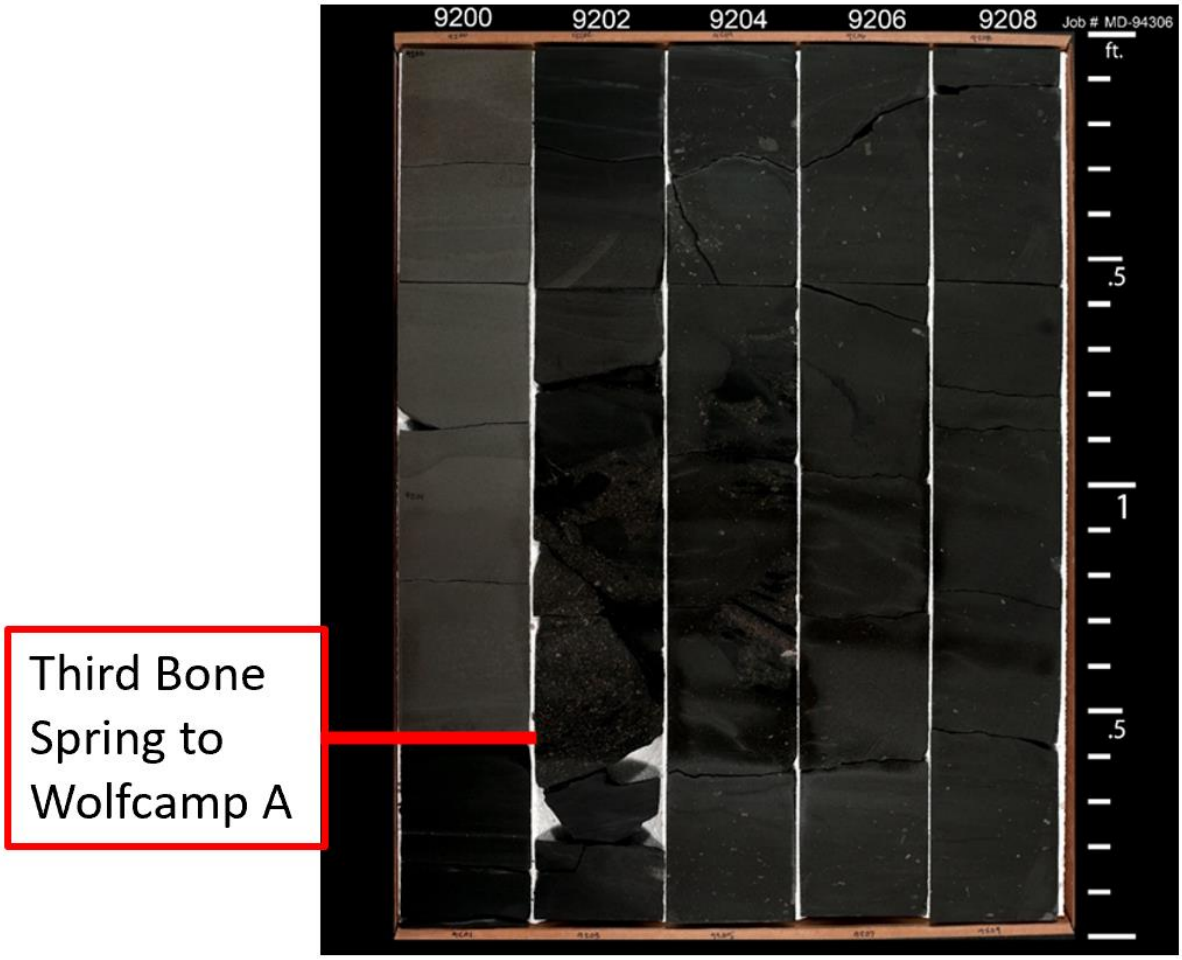

Figure 8. Transition from TBSG to Wolfcamp A in whole core from pilot well.

2.2.2 Minerology

Once the whole core was obtained out of the pilot well, individual samples were taken to determine the mineralogical components of each zone, a key driver in determining hydraulic fracturing ability (Tayler et al., 2013). To do this, core plugs and 200 thin-sections were cut and underwent X-ray diffraction (XRD) and X-ray fluorescence (XRF) analysis to depict each mineral appearing in the core. Due to depth and thickness constraints of the Wolfcamp A-XY, the sample amount was limited to 37 core plugs and 42 thin-sections.

XRD data from the whole core shows that the Wolfcamp A-XY has a simple minerology. From the XRD and XRF analysis, 4 classes (15 individual minerals) of minerals were found present in the Wolfcamp A core (Figure 9). The major groups seen in the XRD data are clay, quartz, and carbonate components. Auxiliary minerals were removed from the analysis due to their combined fraction of less than 2 wt%.

A mineral model was then generated from using the mineralogical components of the core to calibrate to a gamma ray log. This process was performed to add mineralogical value to predict and distribute lithological and correlate missing petrophysical to the 3D geological and geomechanical models. An outline of specific details of the mineral model can be found in Nance and Rowe (2015). Additionally, a synthetic gamma ray log from the core was calculated from an empirical equation in Ellis and Singer (2007), where spectral gamma ray measurements obtain potassium, uranium, and thorium to calculate total gamma ray:

$$Synthetic\ Gamma\ Ray = 16K + 4Th + 8U$$

Potassium (K) in wt%, Thorium (Th) in ppm, and Uranium (U) in ppm.

From the synthetic gamma ray obtained, there is a good match from the amount of each element to the total gamma calculated (Figure 10 and 11). In the model, each of the individual benches are depicted to give a more accurate idea of the reservoir target. Total gamma ray was then compared to mineral classes to show a correlation to each zone. From the Wolfcamp A to the Wolfcamp Y, each of the 5 zones can be seen clearly, along with the identification of the three main lithofacies. The match in the data now gives confidence in using the core data to correlate to a geological model of the reservoir.

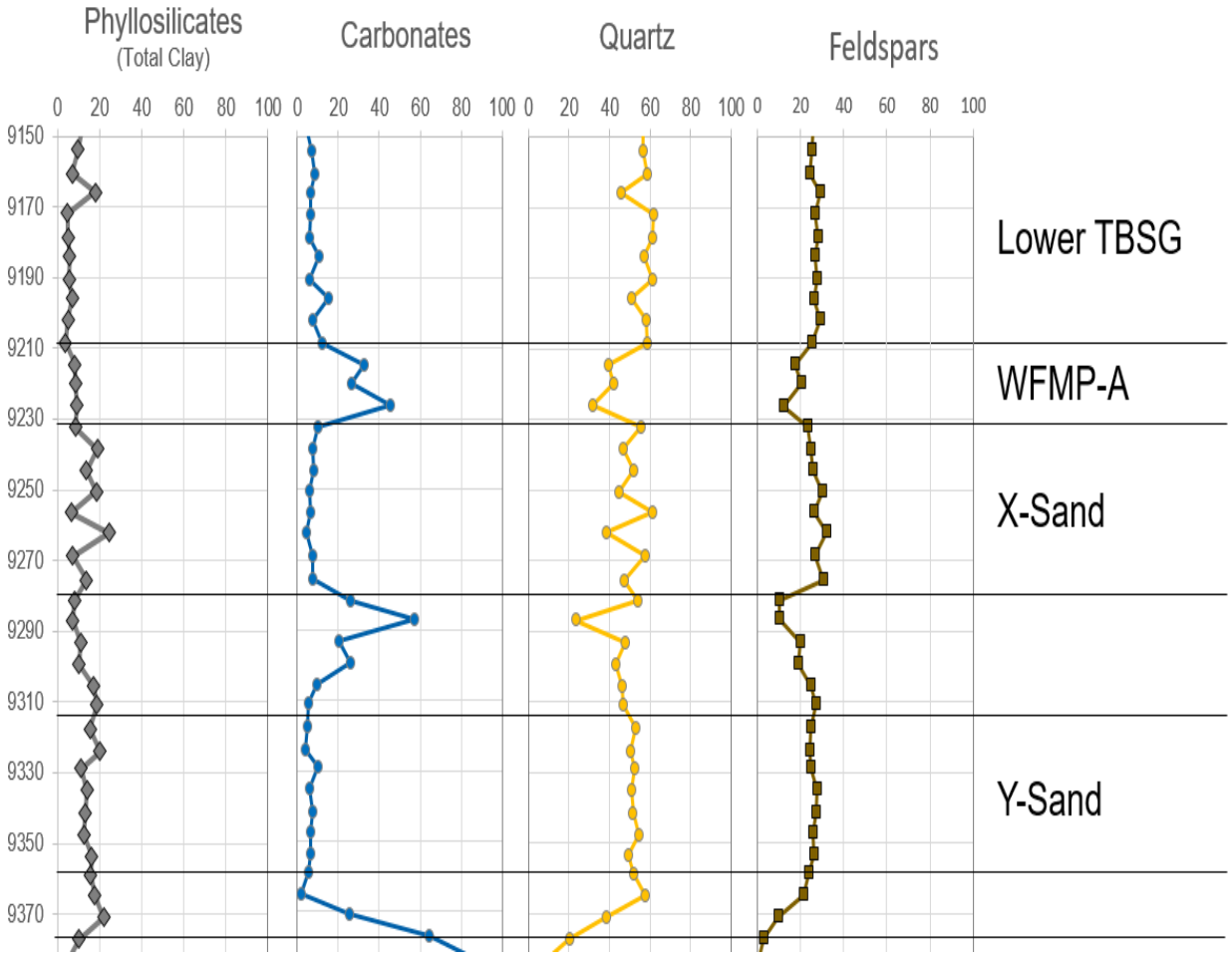

Figure 9. Mineral volumes by percent in whole core for pilot well.

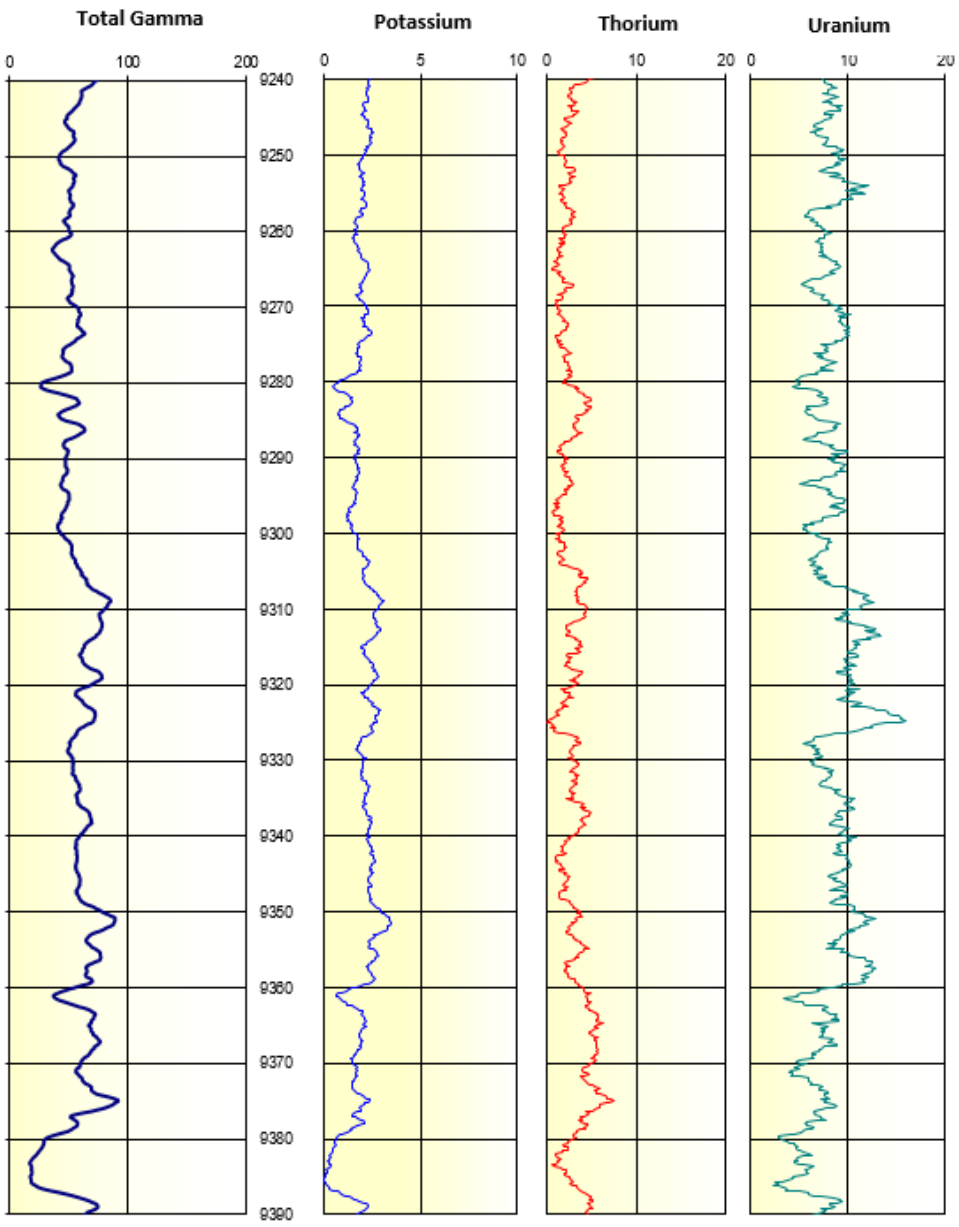

Figure 10. Synthetic gamma ray log determined from empirical equation of potassium, thorium and uranium.

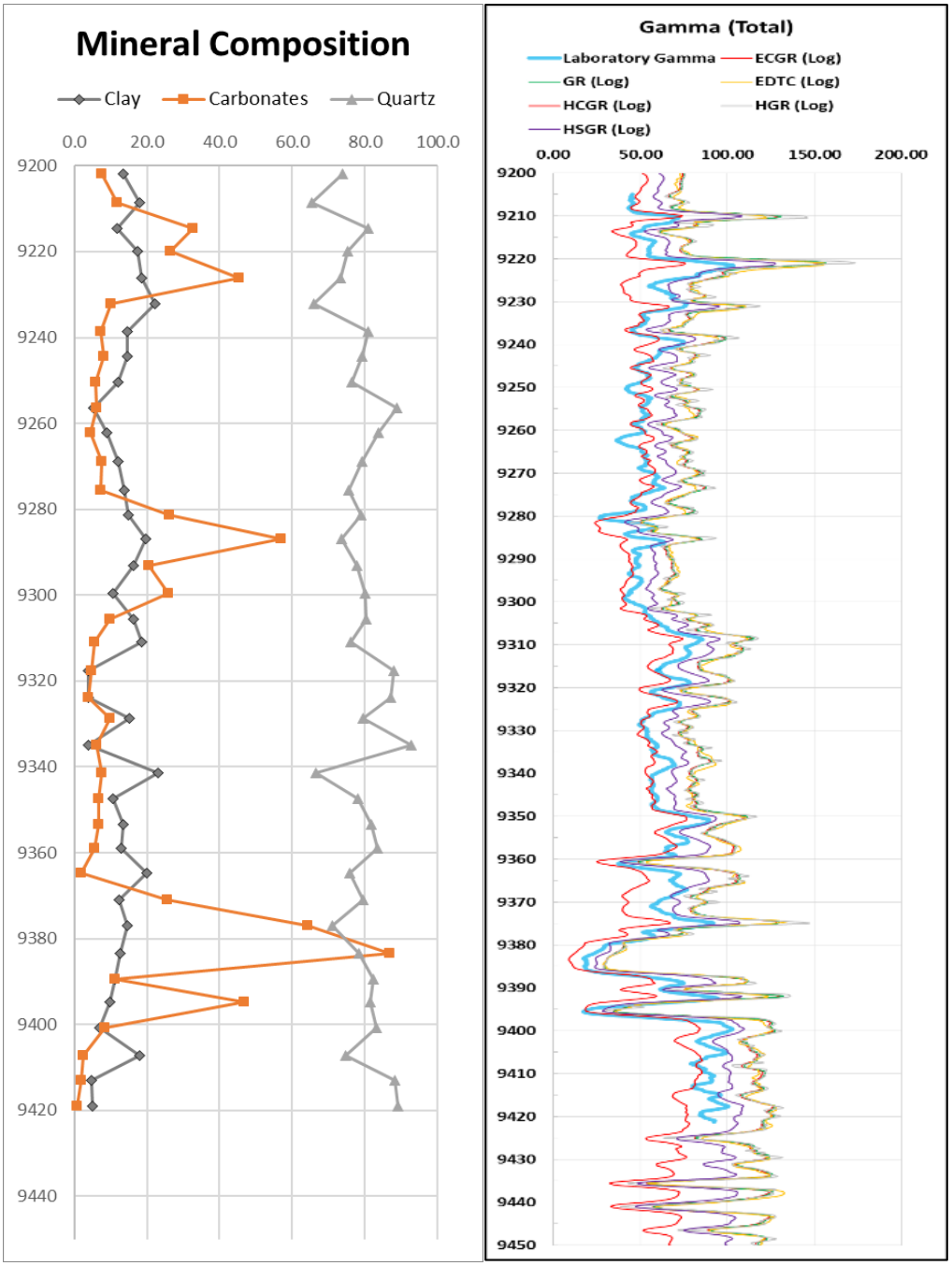

Figure 11. Synthetic total gamma ray log compared to mineral components of the whole core in pilot well.

2.2.3 Petrophysical Properties

A key determination of reservoir characterization workflow is the petrophysical properties of the targeted formations. The Wolfcamp A-XY is an unconventional formation and a very intricate lithology. Analysis from the logs show that the targeted reservoir is chosen by higher gamma ray, porosity, and lower resistivity responses (Malik et al., 2013). Core data determined similar results, with other additional petrophysical rock data. The formation is subdivided into five distinct benches for this analysis, Wolfcamp A, Wolfcamp A-X Upper, Wolfcamp A-X Lower, Wolfcamp Y-Upper, and Wolfcamp Y-Lower.

In order to populate the reservoir model, multiple types of petrophysical rock data needed to be analyzed from the core. Each test method is shown in Table 1. After analysis of each method, an integration of rock types with log and core data aided in the determination of permeability and water saturation transforms. Porosity and water saturation were determined by MICP data along with a comparison with well logs, while permeability was developed with porosity-permeability transforms and being confirmed with MICP data and crushed core analysis. A comparison was made between RSWC porosity and permeability and lithology descriptions, with a high amount of similarity. Figure 12 shows the relationship between porosity and permeability for the pilot well, with each graphical interpretation depicted. Figure 13 shows the measurements of porosity and water saturation from the Dean Stark Technique, while Figure 14 depicts the capillary pressure measurements cross plotted with the wetting phase saturation.

Table 1. Petrophysical property data analysis types performed on crushed whole core of pilot well.

Type	Measurement
Matrix Permeability	Pressure Decay
Fluid Saturation	Dean Stark Technique
Porosity/Grain Density	Boyle's Law Double-Cell Technique
Capillary Pressure/Saturation	Mercury Injection Capillary Pressure

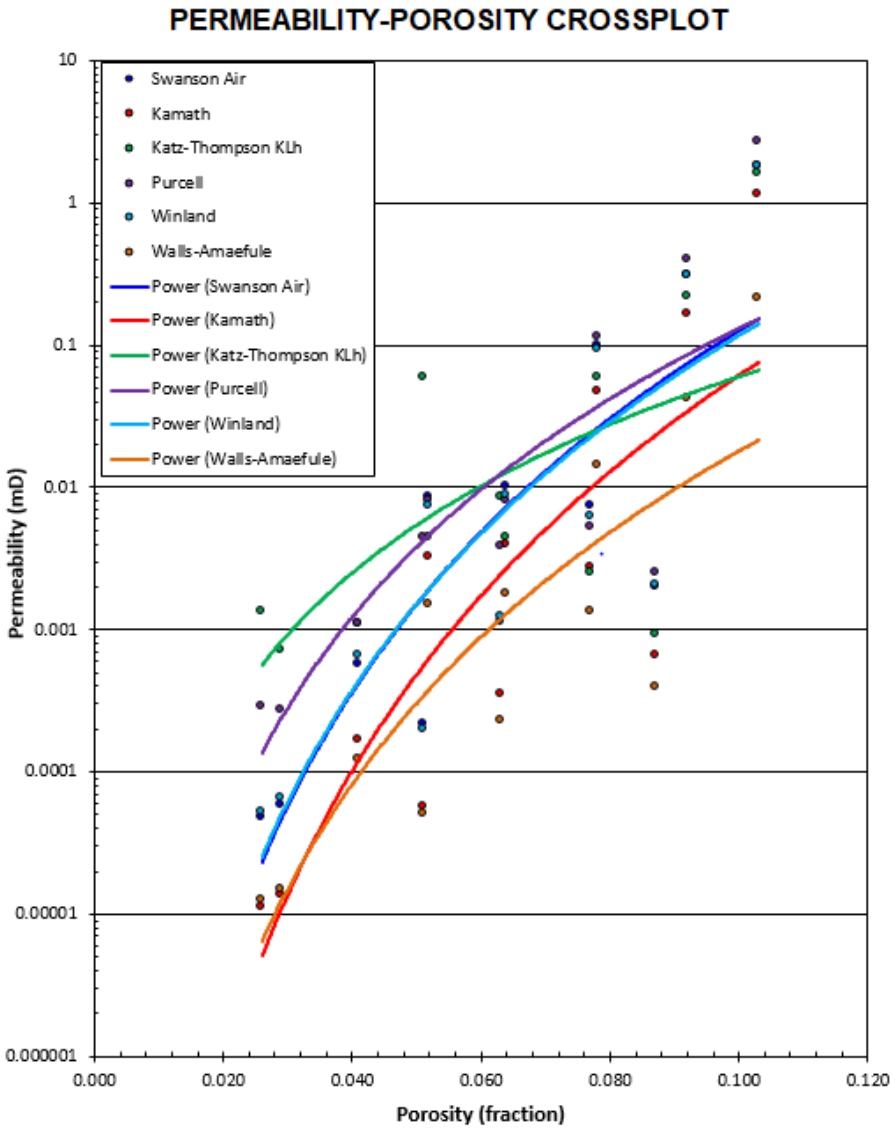

Figure 12. Permeability-porosity cross-plot of crushed whole core in pilot well. Transform equation used as a potential derivation during petrophysical modeling.

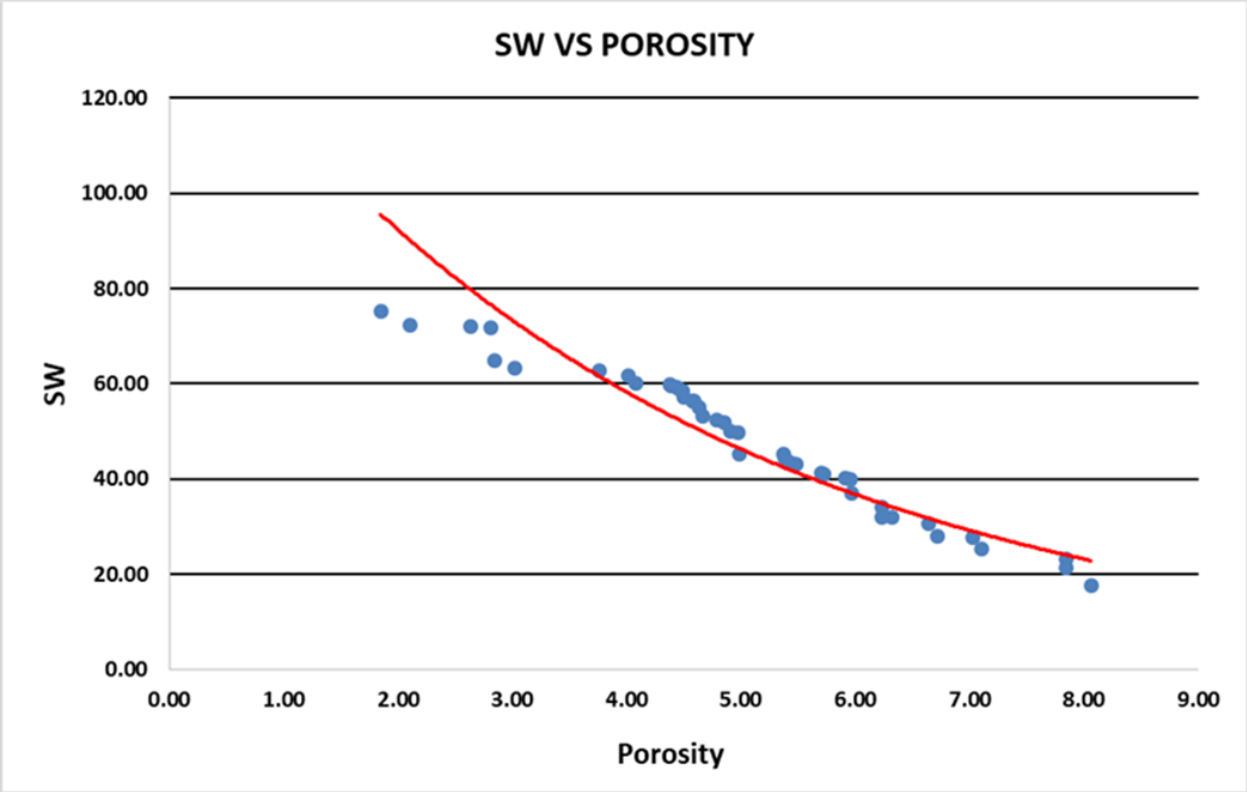

Figure 13. Water saturation and porosity cross-plot from Dean-Stark technique performed on pilot well.

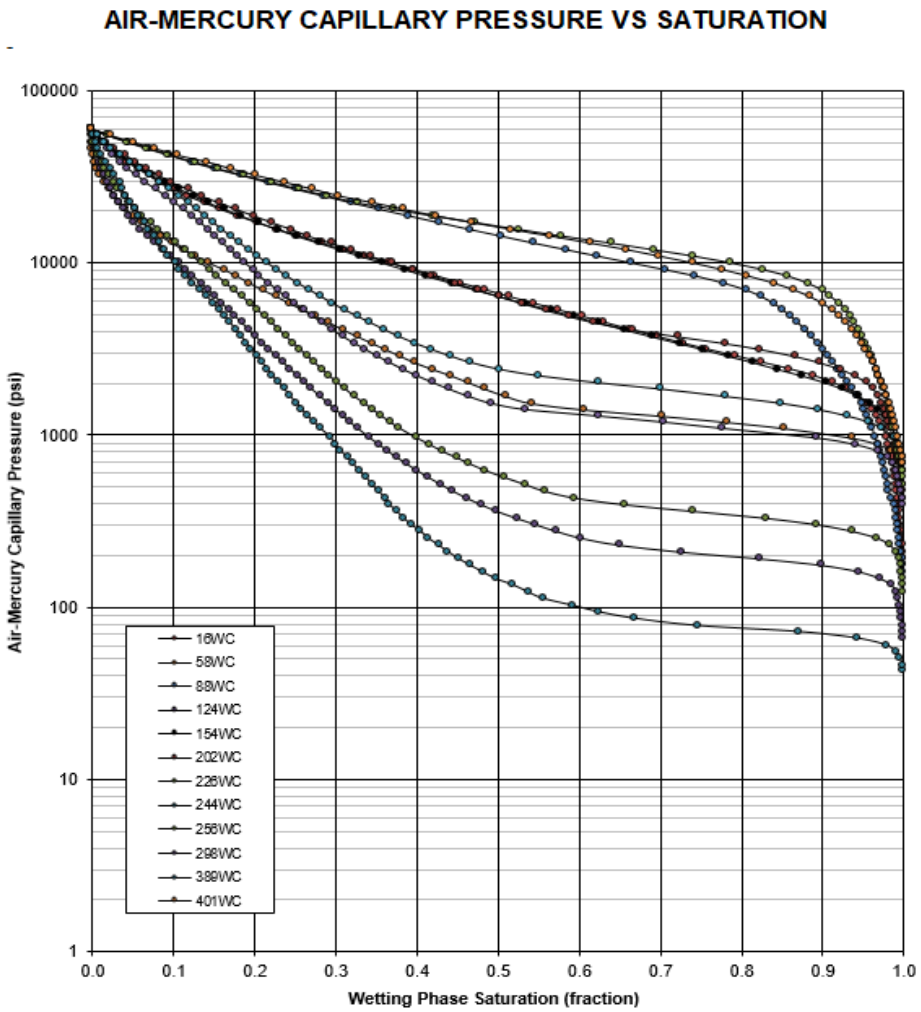

Figure 14. MICP data determining capillary pressure and confirming saturations of whole core in pilot well.

2.2.4 Geomechanical Properties

Geomechanical properties were evaluated from the whole core, RSWC, and a specialized sensor tool called the Fracture-ID. Fracture-ID uses sensors near the drill-bit during the drilling process to measure geomechanical properties of the rock (Haecker et al., 2017). The Fracture-ID tool uses drilling induced vibrations to gather accelerometer, triaxial data to determine these properties in log format. Core testing types are listed in Table 2. The logs displayed in Figure 15 give the output from each test. The first track on the left is SS true vertical depth, the second is

frictional angle, FANG, and the next tracks consist, in order: gamma ray, unconfined compressive strength, tensile strength, Young's Modulus, maximum horizontal strength, minimum horizontal strength, Poisson's Ratio, and vertical stress gradient.

Table 2. Additional core testing analysis types for whole core in pilot well.

Core Testing Types	
Tensile Strength	Brazilian Test
Young's Modulus	Triaxial Test
Poisson's Ratio	
UCS	Brinell Hardness

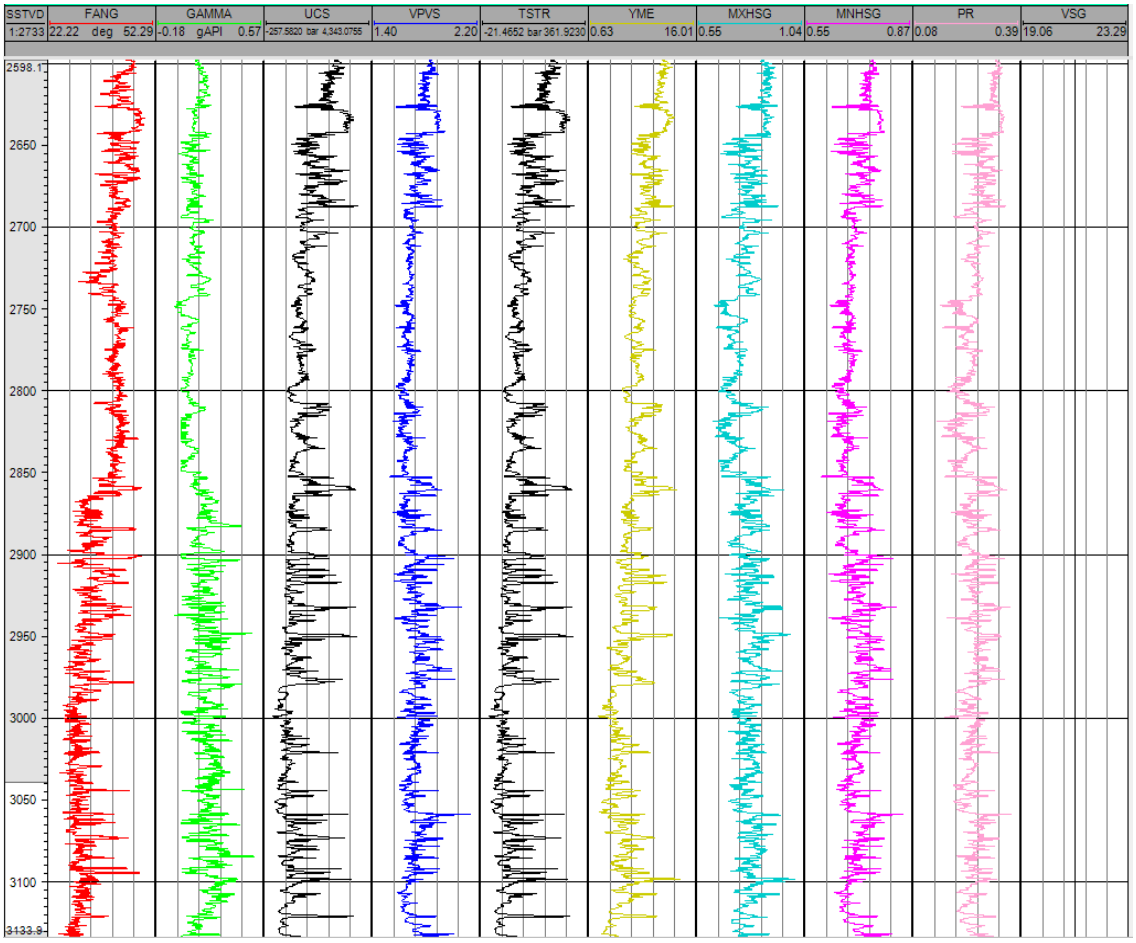

Figure 15. Logs created from core data mechanical properties in pilot well.

2.2.5 Natural Fractures

In order to build the coupled simulation with an accurate 3D geomodel, any natural fracture data needs to be implemented. Even though a core analysis would be able to identify some of the natural fracture network, other methods would be necessary to aid in possible locations along the vertical axis of the reservoir. One of those methods is an FMI log. Due to parts of the proprietary nature of the data used in this study, the FMI log is not shown in the public sphere. However, for geomodelling purposes, the model is populated with data directly from the FMI log.

Chapter 3: Reservoir Characterization and Geological Modeling

Reservoir characterization and populating a geological model is a necessary phase prior to numerical reservoir simulation. This phase is needed to understand the complexity and property distribution of the reservoir. In this chapter, I will explain how I built the geological model for the Wolfcamp A-XY interval used in this study. This includes stratigraphic, structural, petrophysical, mechanical and fluid modeling. The output is that of a 3D geological and geomechanical model that is prepared to undergo simulation analysis.

3.1 Structural and Stratigraphic Modeling

Subsurface well log data comprised from eight wells along with core, fluid, and well log data from the pilot well in the study area was gathered. The well log data includes gamma ray, neutron porosity, sonic, bulk density, density porosity, resistivity, mechanical, and FMI. Core data has been previously stated in this study. However, it includes developing well logs from the core data available and implementing them into the 3D model.

Due to mineralogy being known directly from the core data, a facies model was built from correlations to well log properties, such as bulk density, neutron porosity, and gamma ray. To start, a well log for the pilot well was created for the mineral volumes present in the core, then correlated to a facies determination including sandstone, limestone and shale. Figure 16 shows the depiction of the pilot well log with the corresponding facies, mineral volumes, bulk density, gamma ray, and neutron porosity.

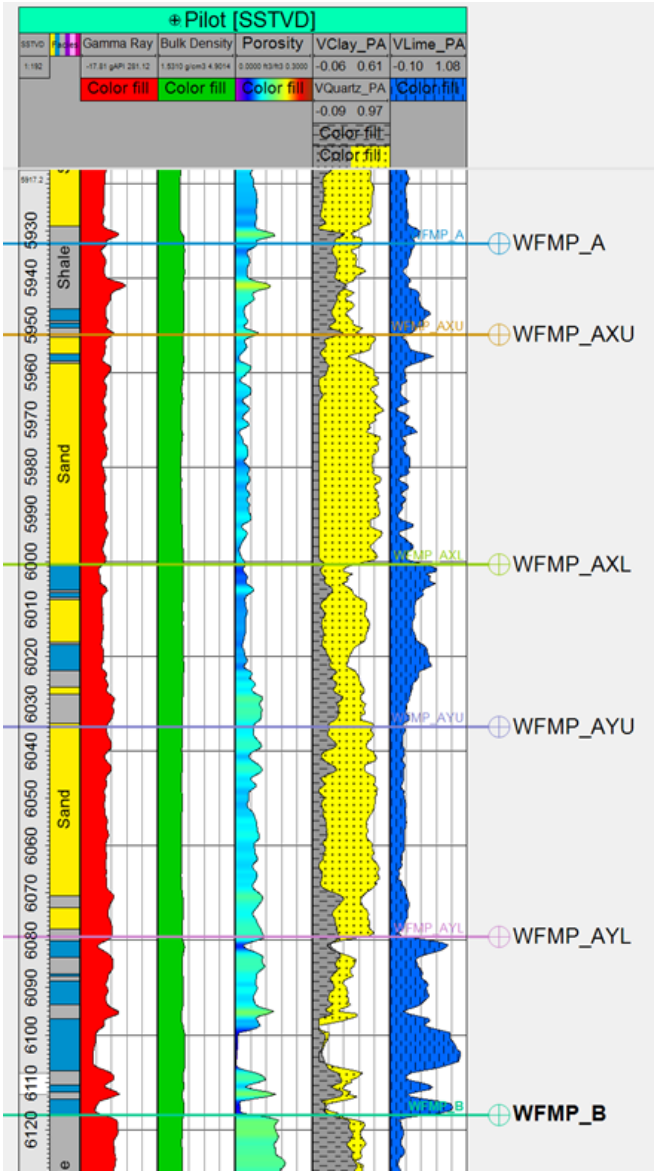

Figure 16. Well log depiction showing gamma ray, bulk density, porosity, mineral volumes, and the well tops for the Wolfcamp A-XY pilot well.

A correlation with all other available well logs was then performed with a neural net, a trend modeling algorithm built in Petrel software, to determine facies for wells without core analysis. Each log was upscaled prior to using Sequential Gaussian simulation (SGS) to build the intervals between each located well in the model. Figure 17 shows the facies distribution inside the geological model with sandstone, limestone and shale.

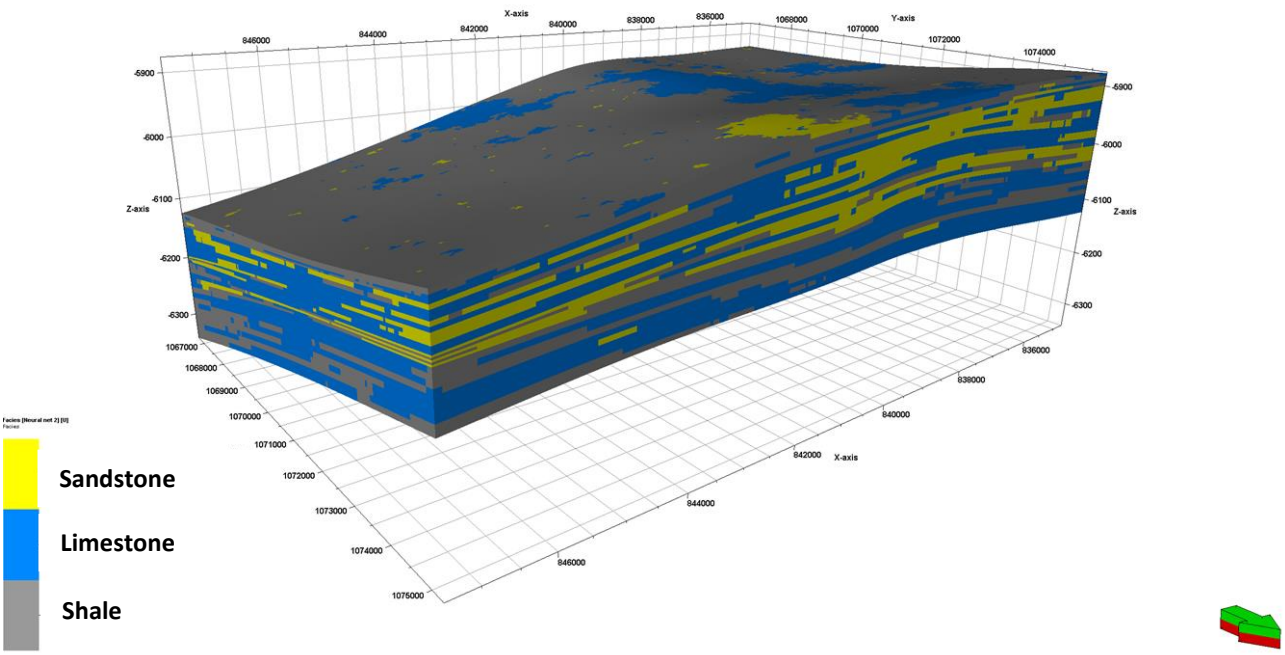

Figure 17. Facies model depicted in 3D for Wolfcamp A-XY focus interval.

3.2 Petrophysical Properties Modeling

In this study, petrophysical properties were determined from core data and correlated to corresponding log data in offsetting wells. These properties are necessary inputs to build a reasonable model for reservoir characterization, hydraulic fracture modeling and production determination and forecasting (Kurtoglu and Kazemi, 2012). Each property was distributed using the Sequential Gaussian simulation (SGS) method. The properties described include porosity, permeability, water saturation, and net-to-gross.

3.2.1 Porosity and Permeability

The Wolfcamp A-XY formation in the Delaware Basin porosity varies between 2% and 12%, with an average of 6%, while permeability can average lower than 1 millidarcy (EIA, 2019).

For porosity, the values for the pilot well with core data were transferred to a log, while neutron porosity, gamma ray, and bulk density logs were used in the software suite Techlog^{TM} to calculate the total and effective porosities (Kilgore, Land, and Schmidt, 1972). Total porosity was determined using grain density of 2.71 g/cm^3 for limestone (ρ_{lim}), 2.65 g/cm^3 for sandstone (ρ_{sand}), 2.61 g/cm^3 for shale (ρ_{shale}), and 2.9 g/cm^3 for dolomite ($\rho_{dolomite}$) (Equation 1). Volume of shale was then determined using gamma ray logs with 100 and 0 as values for max and min values (Equation 2). Finally, effective porosity was calculated using Equation 3 and upscaled to the 3D model with the facies model as a constraint (Figure 18A).

$$\emptyset_T = \frac{\rho_{ma} - \rho_{bulk}}{\rho_{ma} - \rho_{fluid}} \quad (1)$$

$$V_{sh} = \frac{\emptyset_N - \emptyset_T}{\emptyset_{Nsh} - \emptyset_{Tsh}} \quad (2)$$

$$\emptyset_E = \emptyset_T - \emptyset_{Tsh} * V_{sh} \quad (3)$$

For permeability, in Chapter 2, I discussed and showed porosity-permeability transform core data that was taken from the pilot well. For this study, that transform data was used to populate the permeability of the geological model. Figure 18B shows the SGS distribution of the permeability data into the reservoir model.

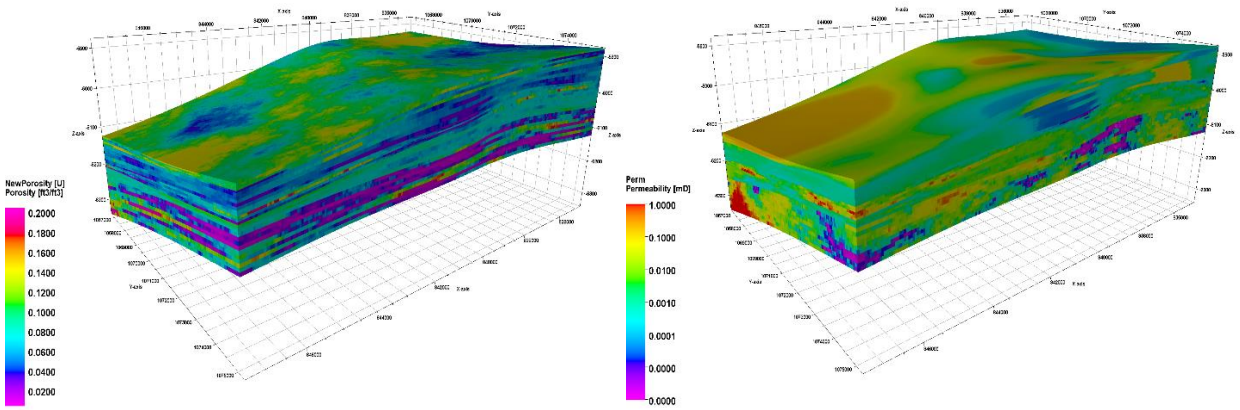

Figure 18. Porosity (A) and Permeability (B) depiction of Wolfcamp A-XY area using core data, well log calculations, and a porosity-permeability transform.

3.2.2 Water Saturation and Net-to-Gross

Two components of the geological model that are necessary to determine in the Delaware Basin are water saturation and net-to-gross. For this study, water saturation was calculated with the Dual Water method to account for clayey sands (Clavier, Coates, and Dumanoir, 1984), and net-to-gross was determined using a Boolean log for net pay cutoffs in the created facies logs and aids in determination of volumetric calculations. To use the Dual Water method, corresponding well logs were imported into Techlog™ and calculated using Equation 4 with all rock types represented (Schlumberger, 2019). Net-to-gross was matched with facies logs as a 0 for non-reservoir, 1 for sand, 2 for shale or clay, and 3 for carbonates. The Boolean log was then used to determine a reservoir cutoff at a porosity of less than 3 percent. The Boolean log uses a true/false logic to determine if something exists in the data or not (Schlumberger, 2018). In short, once the porosity drops below 3 percent, the net pay of that zone goes to 0. Figure 19 shows a 3D depiction of the two properties for the geological model.

$$\frac{a}{(R_t * \emptyset_t^m)} = \frac{1}{R_w} * S_w^n + Q_v * \left(\frac{1}{\emptyset_{tsh}^2 * R_{sh}} - \frac{1}{R_w}\right) * S_w^{(n-1)} \quad (4)$$

$$Q_v = \frac{\emptyset_{tsh} * V_{sh}}{\emptyset_T}$$

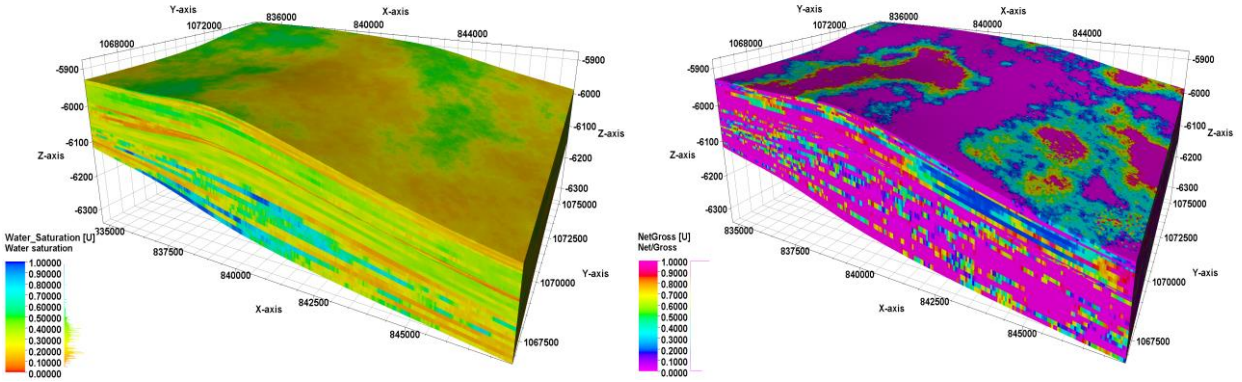

Figure 19. Water Saturation (C) and Net-to-Gross (D) depiction of Wolfcamp A-XY area using core data, well logs, and the Dual Water model.

3.3 Mechanical Properties Modeling

Mechanical, or elastic, properties in unconventional formations are used, as example, to determine the ductility and brittleness of a rock. Young's modulus and Poisson's ratio are the two main properties depicted in this study. In the Wolfcamp A-XY in the Delaware Basin, these properties exhibit variations between intervals due to their mineralogy and lithology (Abouelresh and Slatt, 2011). Determining the values and distribution for each is crucial to the hydraulic fracturing chapter of this study.

To determine the two elastic properties, core data or available bulk density and sonic logs with velocities are necessary. For this study, core data from the pilot well and three available sonic logs, with compressional and shear wave, for offset wells are used. The core data was obtained

from laboratory measurements and plotted in a synthetic well log, while sonic logs were used to derive the elastic properties in the offset wells. The wells without sonic logs were used in Petrel's neural net calculation correlated with porosity, lithology, and water saturation.

To determine compressional (V_p) and shear (V_s) wave velocities, travel times of each were converted to velocities. DTC logs were used to calculate compressional wave velocity, while DTS logs derived shear wave velocity. Equations 5 through 10 were used to calculate compression wave velocity, shear wave velocity, bulk modulus (G), shear modulus (K), Young's modulus (E), and Poisson's ratio (v). Each of these equations were represented in Petrel's Rock Physics calculation plug-in for geomechanics.

$$V_p = \frac{10^6}{DTC} \tag{5}$$

$$V_s = \frac{10^6}{DTS} \tag{6}$$

$$G = \rho_{RHOB} * V_s^2 \tag{7}$$

$$K = \rho_{RHOB} * V_p^2 - \frac{4}{3} * \rho_{RHOB} * V_s^2 \tag{8}$$

$$E = \frac{\rho_{RHOB} * V_s^2 * (3V_p^2 - 4V_s^2)}{(V_p^2 - V_s^2)} \tag{9}$$

$$v = \frac{V_p^2 - 2 * V_s^2}{2 * (V_p^2 - V_s^2)} \tag{10}$$

After deriving each of the elastic properties from the data, a log for each well was created to show the signature of each property (Figure 20). Once they were created, the logs were upscaled, with the facies property as a constraint, and distributed using Sequential Gaussian simulation (SGS). The depiction of the model for Poisson's ratio and Young's modulus are shown in Figure 21.

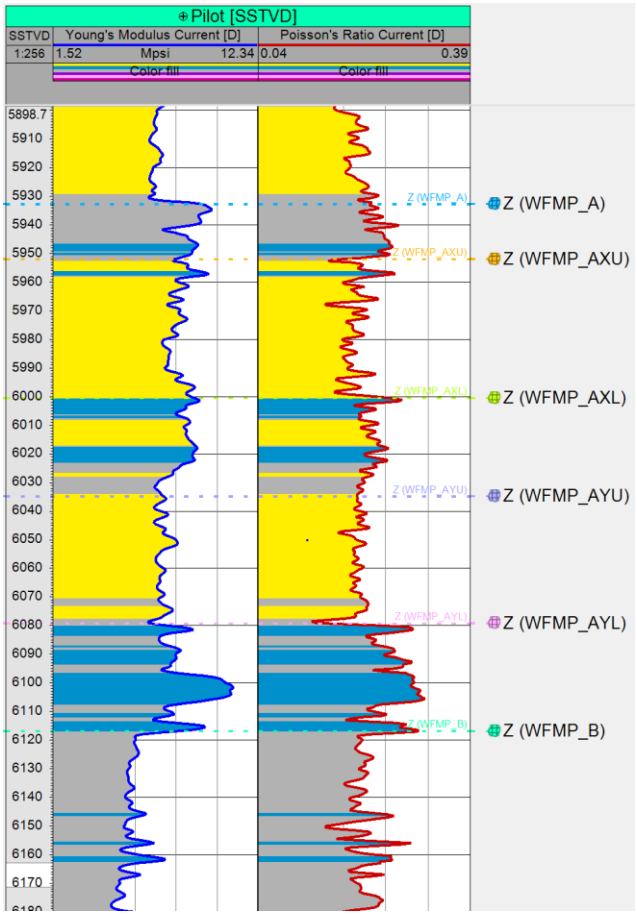

Figure 20. Young's Modulus and Poisson's Ratio logs of Wolfcamp A-XY area using core data, sonic well logs, and the geomechanical calculations.

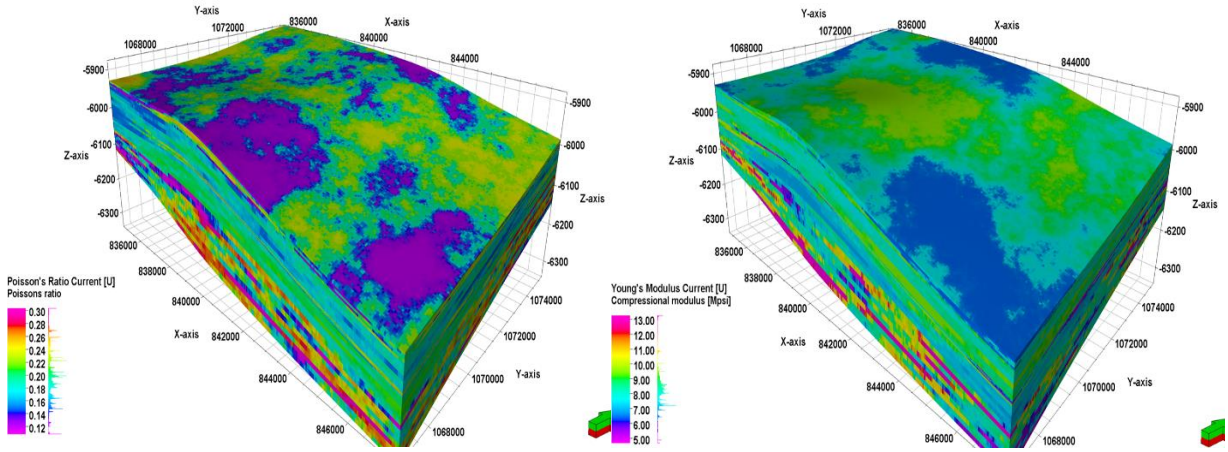

Figure 21. Poisson's Ratio (E) and Young's Modulus (F) depiction of Wolfcamp A-XY area using core data, sonic well logs, and the geomechanical calculations.

Chapter 4: Hydraulic Fracture Model

This chapter focuses on the data and methodology used build a hydraulic fracture model on the development well as the lone well for a development region in the Delaware Basin. The purpose of developing this model is to incorporate it with the coupled geomechanical model discussed in Chapters 2 and 3 to evaluate the resulting hydraulic fracture geometries and characteristics, while history matching the corresponding treating pressure and completion data, then implementing the results into a dynamic flow reservoir simulation. The software used to integrate this model is GOHFER, a commercial 3D hydraulic fracturing simulator. The history match is presented to gain a realistic output of the fractures.

4.1 HFM Grid Properties Modeling

The input data for GOHFER is typically dependent on a large amount of log files. For this study, multiple Log ASCII Standard (.las) files were obtained and used to populate the grid model for the hydraulic fracture design (Barree and Associates LLC, 2017). These logs consist of gamma ray, bulk density, neutron porosity, dipole sonic logs, resistivity, and Fracture ID logs, which were mentioned earlier in the study, with the majority of logs being correlated or created from the previous core analysis.

Once the .las files were processed into GOHFER, log curves were generated, and properties were transmitted into the modeling grid (Barree, 2016). An example of one of these properties is shown, spatially distributed, in Figure 22. Properties brought into the model include effective porosity, permeability, pore pressure gradient, biot's constant, fissure opening pressure, proppant holdup, tectonic stress, transmissibility multiplier, percent rock value, and multiple others described next.

- Process Zone Stress (PZS)
    - This property is a gauge pressure obtained during a fracture injection test that measures initial shut-in pressure, or closure pressure, and extension pressure. PZS doesn't include just one property. Due to the effects of fluid lag, tensile strength, and fracture tip stress changes, it comprises of a combination of all three mechanisms, which can restrict fracture growth. For this property, fracture injection test data was used. No additional calculations were required for population.

- Stress (Total)
    - This is a property taken from the FID log, as well as being calculated using Equation 11 below.

$$P_c = \frac{\nu}{1-\nu}\left[\left(D_{tv}\gamma_{ob} - \alpha_v\left(D_{tv}\gamma_p + P_{off}\right)\right] + \alpha_h(D_{tv}\gamma_p + P_{off}) + \varepsilon_x E + \sigma_l\right.$$

- Poisson's Ratio
    - Due to acquiring a Fracture ID (FID) log during the drilling process, this property is measured, and a calculation is not needed. However, since dipole sonic logs were also obtained, this property was correlated to physical data.

- Young's Modulus
    - Similar to *E*, this property was also measured during the drilling process with the same log type (FID). It was also calculated and correlated from bulk density and dipole sonic logs with core data from the previous analysis.

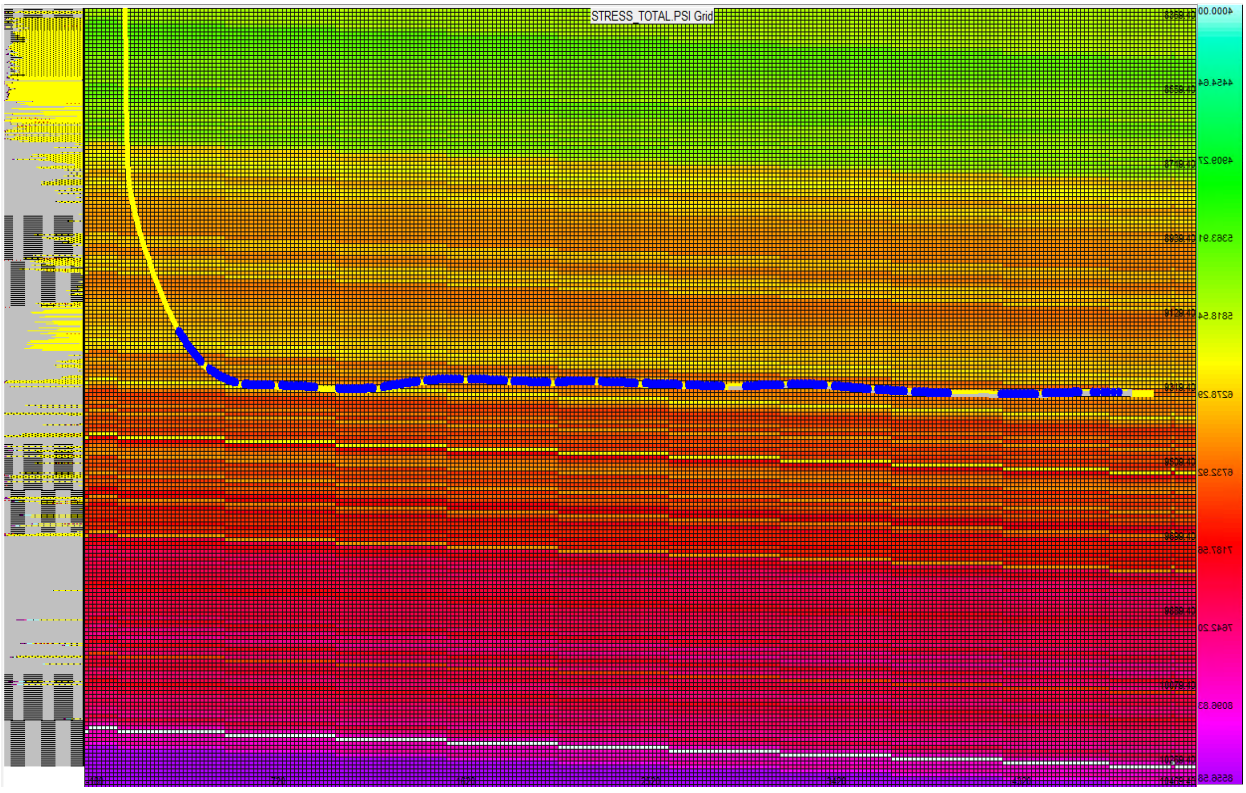

Figure 22. Total stress distribution along the wellbore in a depiction from the hydraulic fracturing model in GOHFER.

4.2 Hydraulic Fracture Treatment Design and Pumping Schedule

The hydraulic fracture treatment on the development well included 22 stages with 6 clusters per stage. Each cluster have a spacing of approximately 35 on average, with a perforation diameter of 0.45 inches. The plug and perf method was utilized to simulate multiple fracture stages simultaneously. For liquids, each stage consisted of a pad of treated water, 2000 gal of 15% HCl, and 400,000 to 450,000 gal of slickwater. For the solid components, each stage consisted of 80,000 to 100,000 lbs of 100 mesh sand and 400,000 to 425,000 lbs of 40/70 proppant. Additional, undisclosed to this study, chemicals were added to mitigate potential swelling and wellbore issues during the completion. The pumping schedule for a single stage is shown, in detail, in Table 3, while a graphical depiction of actual treating pressure and pumping rate is shown in Figure 23. Additional inputs included pressure-dependent leakoff (PDL) coefficient to determine the surplus of leakoff with the opening of natural fractures, the perforation coefficient of discharge to determine perforation friction, pressure dependent modulus stiffness factor (MSF), tubing diameter and current wellbore fluid.

Table 3. Observed pumping schedule for development well for 22 stages of design.

Stage #	Stage Time	Fluid Type	Clean Stage Vol (GAL)	Proppant	Slurry Conc (PPA)	Slurry Rate (BBL/min)	Clean Fluid Rate (BBL/min)
1	1:09	Treated Water	338.1	<None>	0	7	7
2	2:04	HCl_15%	920.08	<None>	0	10.6	10.6
3	21:38	SlickWater	15446.2	<None>	0	17	17
4	5:07	SlickWater	14873.79	100 Mesh Sand	0.25	70	69.21
5	4:47	SlickWater	17069.83	100 Mesh Sand	0.5	86.9	84.97
6	7:15	SlickWater	26299.6	100 Mesh Sand	1	90.3	86.37
7	6:40	SlickWater	23615.94	Atlas PRC-E 40/70	1.25	89.3	84.34
8	6:47	SlickWater	24084.71	Atlas PRC-E 40/70	1.5	90.5	84.54
9	8:01	SlickWater	28185.7	Atlas PRC-E 40/70	1.75	90.6	83.71
10	9:51	SlickWater	34145.94	Atlas PRC-E 40/70	2	90.3	82.54
11	6:47	SlickWater	22405.76	CarboProp 40/70	2	84.4	78.64
12	0:50	RheoGel	1197	<None>	0	34.2	34.2
13	6:00	SlickWater	8618.4	<None>	0	34.2	34.2
14	5:33	SlickWater	10069.93	<None>	0	43.2	43.2
15	3:23	SlickWater	12406.29	100 Mesh Sand	0.25	88.3	87.31
16	4:44	SlickWater	17571.71	100 Mesh Sand	0.5	90.4	88.39
17	6:42	SlickWater	24331.36	100 Mesh Sand	1	90.4	86.47
18	4:59	SlickWater	17870.35	Atlas PRC-E 40/70	1.25	90.4	85.38
19	6:24	SlickWater	22698.55	Atlas PRC-E 40/70	1.5	90.4	84.44
20	8:21	SlickWater	29325.25	Atlas PRC-E 40/70	1.75	90.5	83.62
21	8:46	SlickWater	30424.11	Atlas PRC-E 40/70	2	90.4	82.63
22	5:24	SlickWater	20511.62	CarboProp 40/70	0	90.3	90.3
23	10:49	SlickWater	36662.06	<None>	0	80.7	80.7

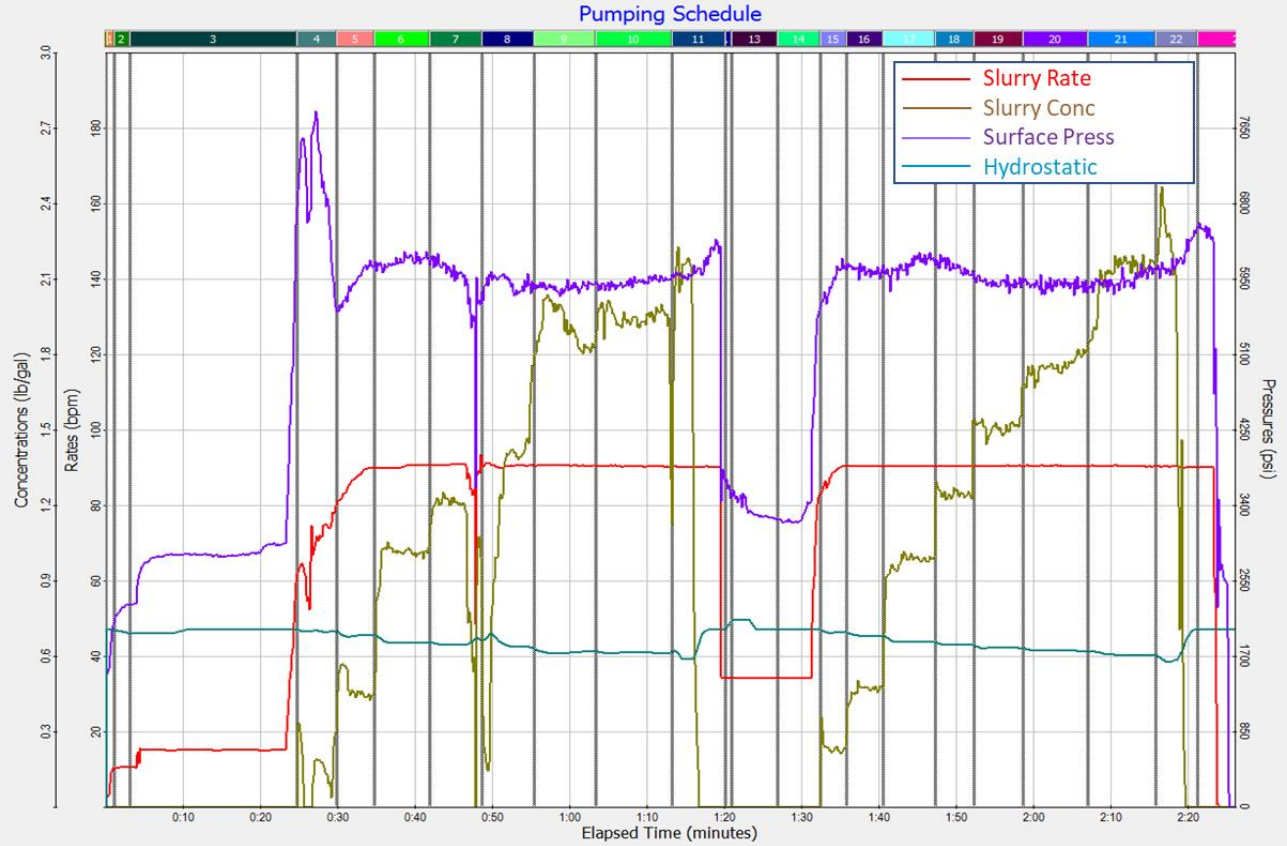

Figure 23. Graphical depiction of pumping schedule for 1 stage of the 22 stages.

4.3 Hydraulic Fracture Simulation Results

Figure 24 shows the output from one stage of the simulated hydraulic fracture model. In blue is the simulated surface pressure compared to actual surface pressure data in purple. This matching was performed for each of the 22 stages of the model. The resulting data for fracture geometries is shown in Table 4. For the average case, each zone is specified, along with fracture half-length, width, proppant concentration, and conductivity.

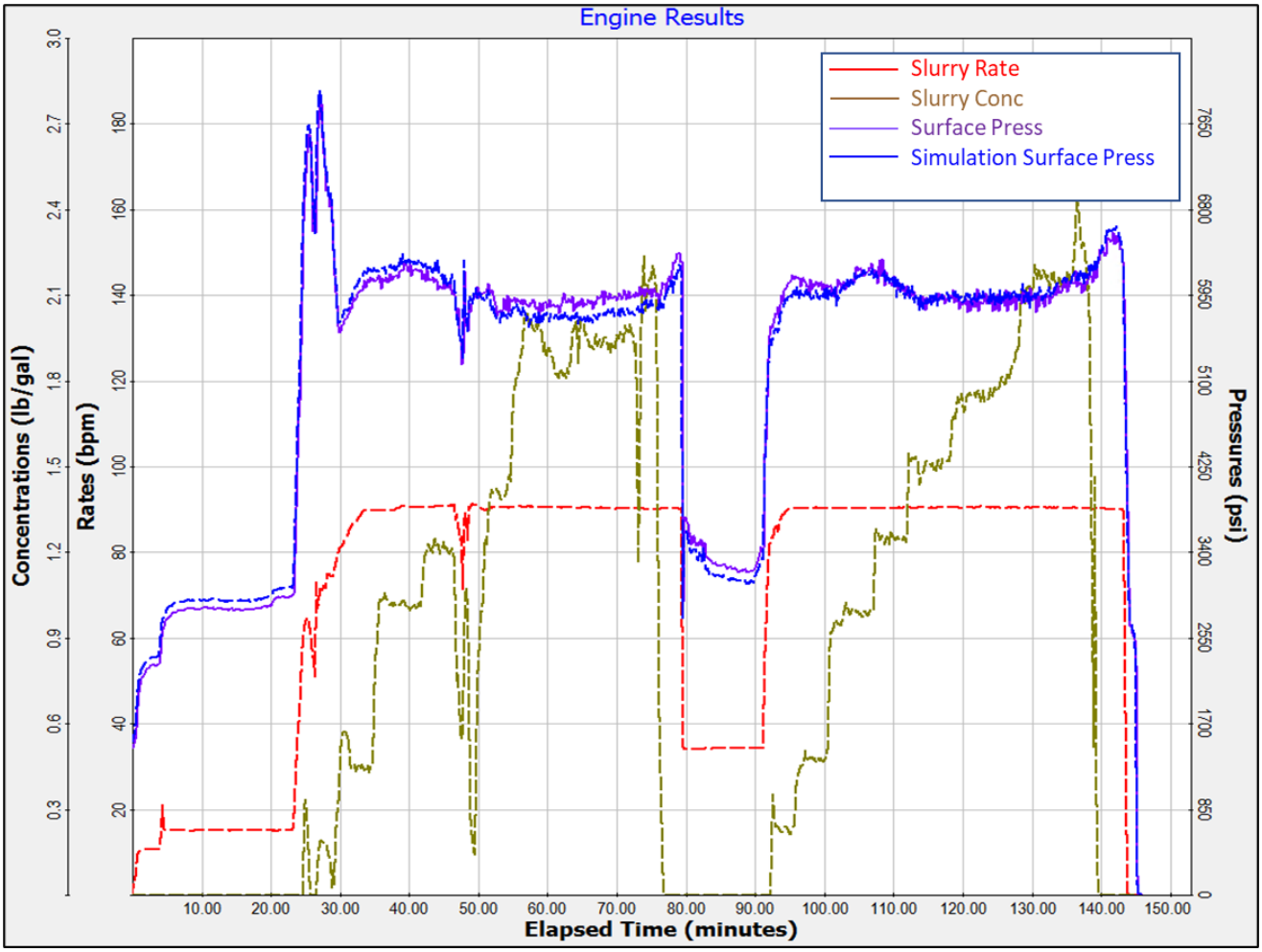

Figure 24. Treatment pressure match for one stage of hydraulic fracture design.

Table 4. Average hydraulic fracture geometries for each zone in the wellbore simulation.

Average Hydraulic Fracture Geometry Values					
Zone	Propped Fracture Half-Length (ft)	Propped Fracture Height (ft)	Proppant Conc. (lb/ft^2)	Width of Fracture (in)	Fracture Conductivity (md-ft)
Wolfcamp A	186.40	17.20	0.18	0.30	43.62
Wolfcamp AXU	352.30	29.22	0.25	0.19	19.52
Wolfcamp AXL	522.90	32.40	0.31	0.17	21.30
Wolfcamp AYU	603.30	48.99	0.32	0.22	56.65
Wolfcamp AYL	623.60	51.20	0.45	0.23	69.17

After simulation of the 22 stages of hydraulic fracturing, an output file was created with direct points that are populated with the attributes in Table 4. One constraint of this model is to focus the fractures only in the Wolfcamp A-XY. This is due to multiple wells currently producing in a shallower formation approximately 200 feet above this well not seeing a large impact on production or pressure in the early data. This does not suggest that the fractures will not extend into the shallower formation. The file represents the exact dimensions of the geomechanical earth model created in prior chapters. Once created, the points were imported and upscaled to properties in the reservoir simulator (Phan et al., 2018). Figure 25 shows the point set in the grid, while Figure 26 shows the upscaled properties created from these points.

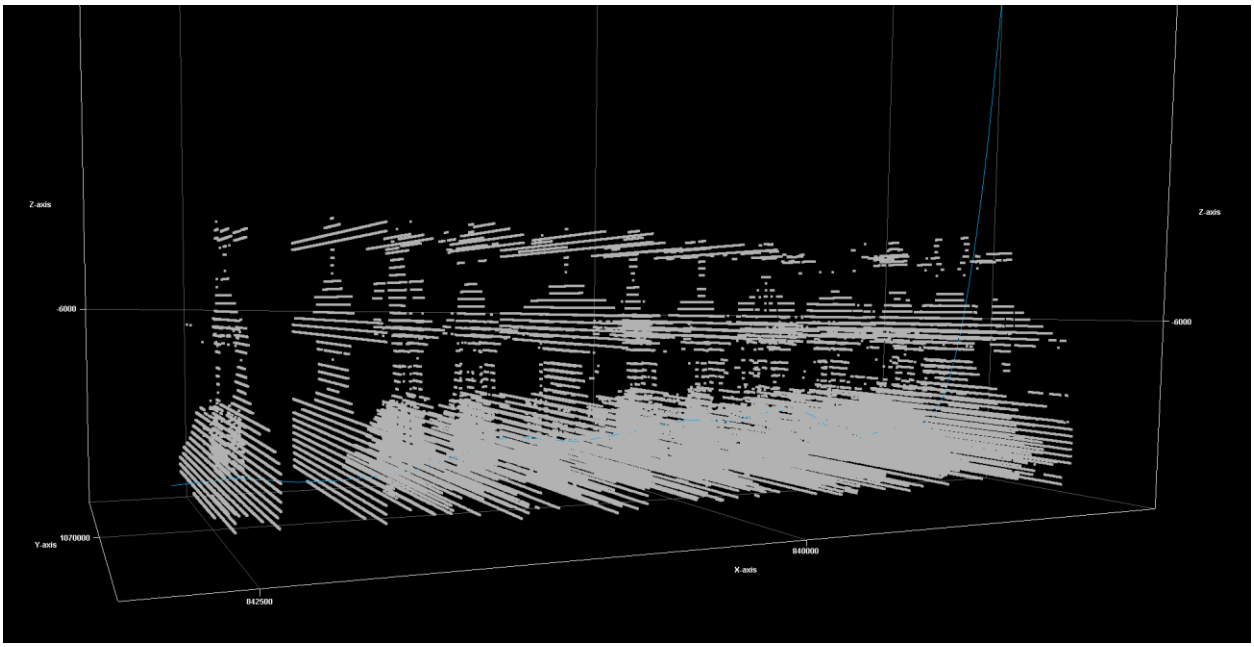

Figure 25. Point data imported as attributes into the 3D geological grid.

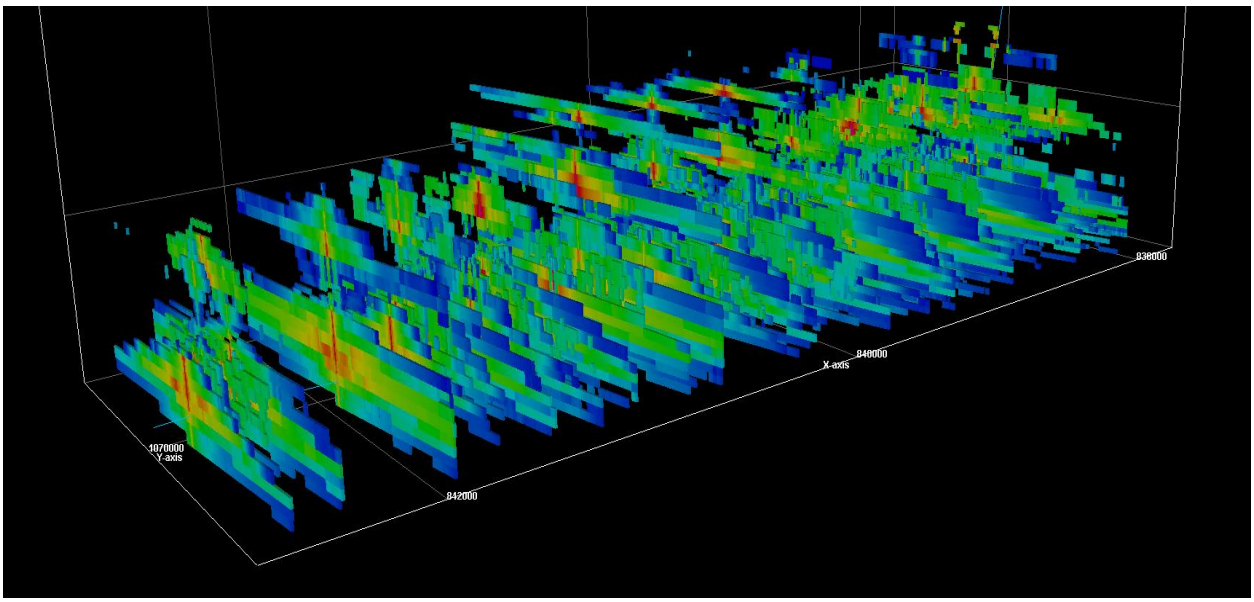

Figure 26. Upscaled depiction of point data into petrophysical transmissibility properties.

Chapter 5: Reservoir Simulation

This chapter focuses on the data implementation and methodology used in the framework of the integrated numerical reservoir simulation. The combination of the geological and mechanical earth model in Chapter 3 and the hydraulic fracture design in Chapter 4 are used to evaluate the production performance of the life of the development well. The reservoir simulation software used in ECLIPSE™. Later parts of the chapter present results for the base case of the well.

5.1 Simulation Model

The reservoir model built in Chapter 3 was described as a dual porosity model. Due to this, multiple properties, including permeability and porosity, are split between the matrix and natural fracture network. The 3D grid that is the basis for the reservoir model was reduced to a smaller model, originally approximately 5 million 50x50 cells, down to a model of 109x125x30 cells (1 x 0.4 miles). Properties for the fracture network, both natural and hydraulic, were implemented into the model.

As discussed in Chapter 3, the natural fracture network was populated via SGS. For the hydraulic fracture model, points were imported into the 3D grid from GOHFER, as discussed in Chapter 4. However, due to the natural fracture network already implemented, the hydraulic fractures were modeled through transmissibility multipliers (Barree, 2016). Figure 26 in Chapter 4 depicts the 3D model focusing on the upscaled property for the hydraulic fracture network. Closer to the wellbore has a higher multiplier with warmer colors and, as distance is covered, a lower multiplier with cooler colors.

For the properties outstanding, Table 5 summarizes these at a relation to the data retrieved from field estimates.

Table 5. Reservoir initial input data for simulation from field estimates.

Input	Initial Value
Reservor Pressure, psia	4067
Water Saturation, %	35%
Temperature, ^{o}F	145
Depth, ft	6000
GOR, scf/bbl	2300
WOC, ft	6250
Tubing Depth, ft	8600

5.2 Compositional Fluid Model and Relative Permeability

Prior to determining the output from any reservoir simulation model, one must acquire a reservoir fluid data sample that is representative of the fluid at initial conditions to assess the behavior of the fluid during the production life of the well. This data can be simulated as a black oil or compositional fluid (Aziz and Settari, 1979). However, due to the lack of changing fluid output with a black oil model, a compositional fluid model is necessary.

In this study, separator samples of both gas and oil were mathematically recombined, at reservoir conditions, to form the compositional fluid model imported from CMG's Winprop into the reservoir simulation. The separator conditions were measured at 400 psig and 107 F. The fluid composition of each stream is comprised of twelve components and one pseudo-component. The fluid has a saturation pressure of 2750 psi and API gravity of 42 at a gas-oil ratio (GOR) of 2500

mcf/bbl. Table 6 shows individual components, while Figure 27 depicts a phase envelope for the recombined fluid.

Table 6. Recombination of components from separator values in Winprop.

HC Liquid	
Component	**Mol%**
Nitrogen	0.063
Carbon Dioxide	0.02
Methane	8.794
Ethane	7.84
Propane	9.639
Isobutane	2.081
n-Butane	6.53
Isopentane	2.887
n-Pentane	3.752
2,2 Dimethylbut.	2.25
n-Hexane	2.213
Heptanes Plus	53.93

HC Gas	
Component	**Mol%**
Nitrogen	1.225
Carbon	0.113
Methane	76.534
Ethane	13.615
Propane	5.598
Isobutane	0.569
n-Butane	1.333
Isopentane	0.245
n-Pentane	0.277
Hexanes	0.211
Heptanes Plus	0.28

Recombination	
Component	**Mol%**
Nitrogen	0.96
Carbon Dioxide	0.09
Methane	60.88
Ethane	12.28
Propane	6.53
Isobutane	0.91
n-Butane	2.53
Isopentane	0.86
n-Pentane	1.08
n-Hexane	1.19
Heptanes Plus	12.68

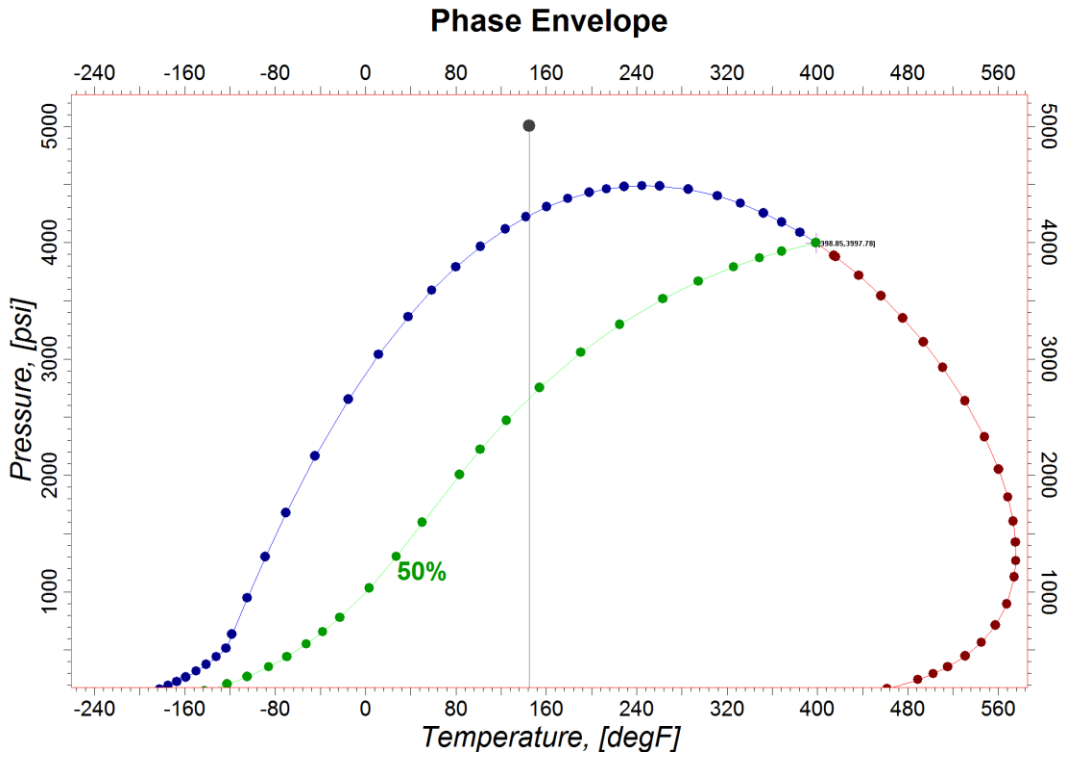

Figure 27. Phase envelope for the resulting compositional fluid model.

Due to the reservoir being configured as dual porosity, two relative permeability systems were implemented. The main system was that of the Wolfcamp A-XY matrix. For this curve, points were implemented into the reservoir model from works focused on core (Ojha et al., 2017). The output of saturation points and Corey exponents is shown in Figure 28, as well as Table 7. For the natural fracture network, relative permeability curves were generated using a correlation following Corey's linear pattern.

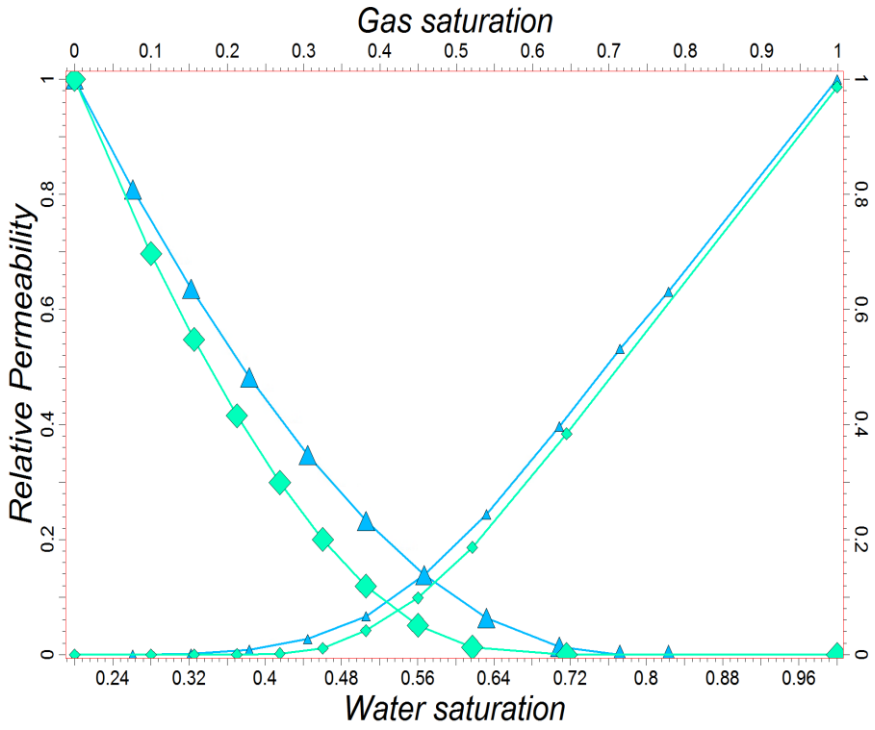

Figure 28. Relative permeability estimates recreated from Ojha et al., 2017.

Table 7. Relative permeability endpoints and Corey exponents from Ojha et al., 2017.

Input	Matrix	Fractures
S_{orw}	0.25	0.25
S_{gcrit}	0.1	0.1
S_{wcrit}	0.35	0.35
k_{rocw}	1	1
k_{rwiro}	1	1
k_{rogcf}	0.7	0.7
Corey oil	3	1
Corey gas	6	1
Corey water	4	1

5.3 Base Case Simulation Results

The Base Case was evaluated for 17 years with a bottom hole pressure (BHP) limit of 500 psi and a total liquid rate at a maximum of 500 barrels per day (BPD). For this case, the well production declined at a rate similar to that of unconventional formations (Holanda and Valko, 2018). Figure 29A and Figure 29B show the 17-year rates for oil and gas, as well as component flow and bottom hole pressure for the Base Case. As the well reaches the BHP limit quickly, production declines sharply within the first year, as GOR only fluctuates at approximately the same value. Component rates decline at similar rates as the oil and gas rates. Figure 30 shows each of the production for the components from the fluid model described earlier in this chapter. As one can see, the production rates are highest with the most abundant components and lowest with the least abundant components, going from C1 (highest) to CO_2 (lowest).

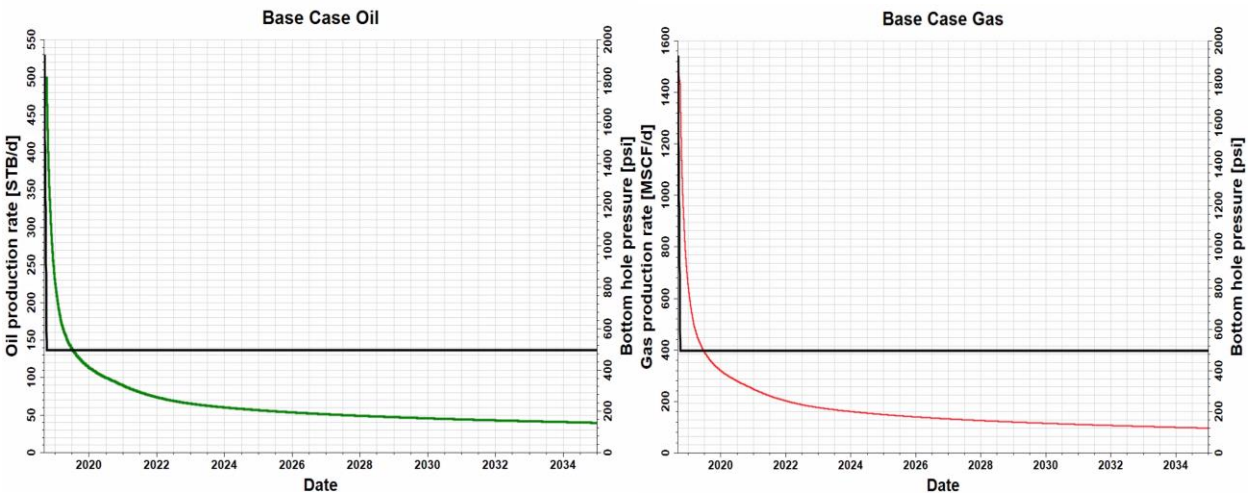

Figure 29. (A) Base Case oil production rate over 17 years. (B) Base Case gas production rate over 17 years.

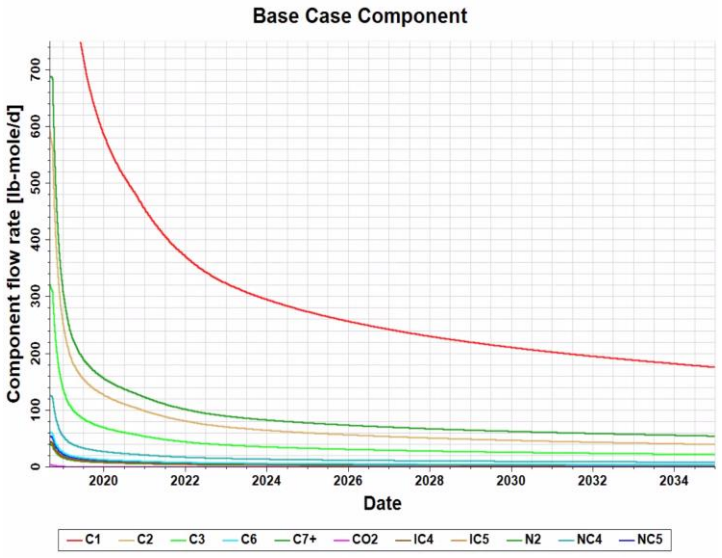

Figure 30. Compositional production rate during the 17-year Base Case.

After the base case was completed, a brief sensitivity study was conducted on the resulting output of the 3D model for cumulative oil and C7+ components to aid in the prediction and accuracy of the base case simulation model. Sensitivity analysis can aid in determining the parameters with the greatest effect on an objective function inputted in the simulation. This study can also help in a history matching process for future studies on this well and field. For this study, seven independent variables were used with a range of multipliers of 50 percent to 150 percent. To be clearer, the minimum value used was 50 percent of the original 3D model input value and a maximum of 150 percent of the 3D model input value. These inputs can give a wide range of results while providing a more systematic result for sensitivity. Also, for each variable, the minimum and maximum values are found as similar bounds in the 3D model (Spaid et al., 2016). For example, the average water saturation is 35 percent in the 3D model. However, the minimum value found nearest the producing well was 18 percent, similar value to the minimum range value. The maximum value follows the same logic. After looking at each of the values and adjusting for relevance, a tornado chart, shown in Figure 31, depicts the 50-150 percent range.

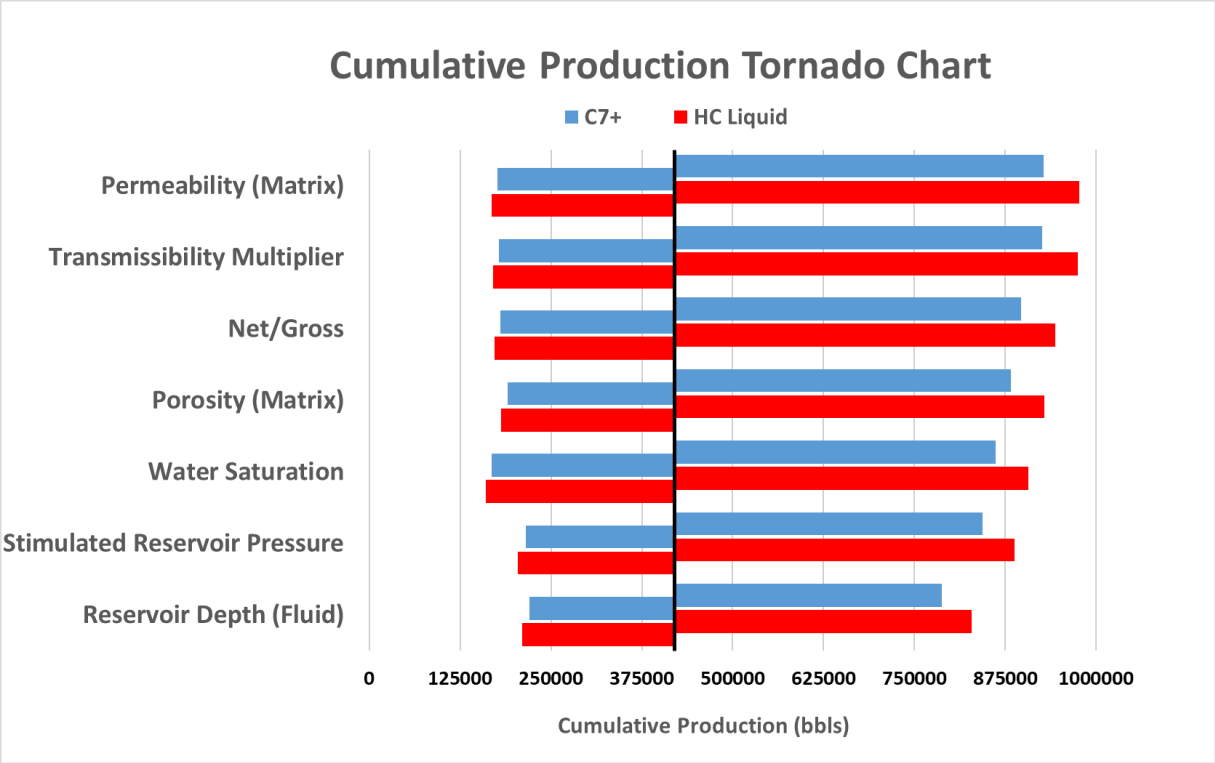

Figure 31. Tornado plot for sensitivity analysis of parameters in the base case model for the original 3D model.

From the tornado plot, the highest impact variables in the 3D model and simulation are matrix permeability and the transmissibility multiplier used for the hydraulic fracturing model. The five remaining give an idea of the impact of each corresponding variable. This plot shows the relative importance of each input variable in the overall error of a history matched model (Victorino et al., 2016). A process that will be completed in a following study.

Chapter 6: Miscible Gas Injection Simulation

In the lifecycle of most wells, a need for new and improved recovery mechanisms will keep the well both producing and economical. Some of the simplest methods for improved recovery are waterflooding, gas injection, and thermal recovery. Due to the reservoir being unconventional,

the permeability is too low to use water flooding and thermal recovery projects require much more difficulty with setup (Elhajjaji et al., 2017). So, for this study, the method of choice is that of miscible gas injection. Preferably with the huff-n-puff setup.

In this thesis, we studied the use of cyclic gas injection in order to achieve a degree of miscible displacement to improve recovery and sweep efficiency in the reservoir. In the miscible displacement process, the injected fluid reaches a pressure at the reservoir to become miscible, or mix, with the reservoir fluid, eliminating the interfacial tension (Salman et al., 2019). This process was implemented prior to the injection periods. The two most available gasses used are lean hydrocarbon gas (HC Gas) and carbon dioxide (CO_2) (EIA, 2020). In the lean gas injection case, the produced gas from a field adjacent to this one will be used to reinject back into the reservoir at this well point. For the CO_2 case, a volume of gas with pure component will be injected. For each of these cases, we used the same injection rate for 3 cycles each. Figure 32 below illustrates the huff-n-puff process in the study's miscible gas injection model.

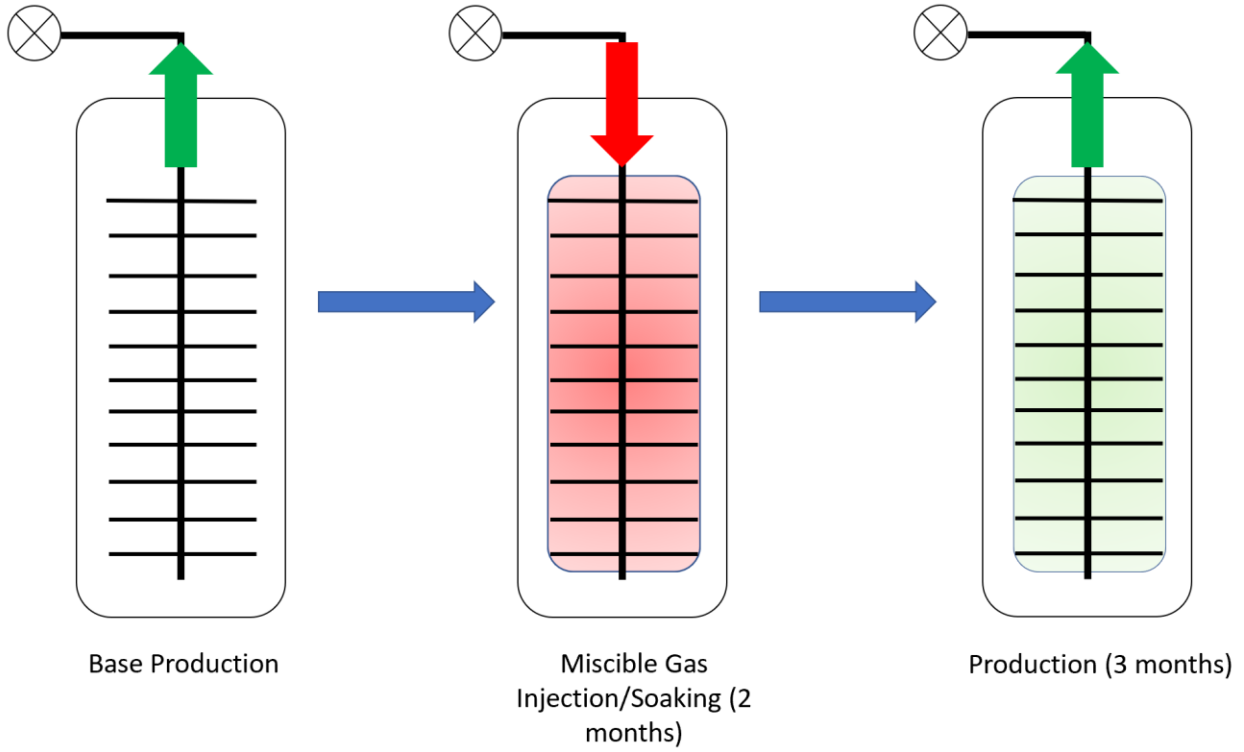

Figure 32. Illustration of cyclic injection strategy for EOR miscible gas injection.

To model the miscible gas injection model, I implemented the unconventional geological model with the horizontal, hydraulically fractured well completed in the Wolfcamp A-XY presented in the prior chapters. ECLIPSE compositional simulator was implemented with a dual-porosity model to simulate both the matrix and natural fractures. Due to molecular diffusion being the main recovery mechanism for cyclic EOR, those values were set at 3.2×10^{-13} for CO_2 and 4×10^{-14} m^2/sec for HC Gas (Zhang et al., 2017). As one can see from the illustration above, the model starts out with producing from the base case all the way until the well is starting to show declination in reservoir producibility. Then, the miscible gas is injected for 1 month, 1 month of soaking, and finally a 3-month window of commencing production. This process is implemented

only 3 times, or 3 cycles, throughout the life of the well. Each cycle is back-to-back to reduce the time it takes to simulate the large model.

The simulations also come with multiple assumptions discussed in prior chapters. A few of the main ones are necessary to communicate. The first is that the core data taken from the pilot well can be correlated to the additional 7 wells located in the study region. This affects all petrophysical data, including porosity, permeability, elastic parameters, natural fracture data from FMI logs, saturation profiles, and lithology. The second main assumption focuses on the homogeneity of component location across the study region. In short, the simulation model assumes compositional volume is the same or similar across the study reservoir.

In order to cover a broad range of simulation cases, 32 individual cases, intermixed with the base case model, hydrocarbon gas injection model, and the CO_2 injection model underwent analysis to acquire uncertainty and sensitivity measurements of each EOR miscible injection process and the time of implementation of each. The results of these cases are summarized in sections following.

6.1 MMP Determination

Determining the minimum miscibility pressure (MMP) is a necessary process in miscible gas injection prior to simulation. Usually, correlations are used to determine MMP without lab results and field projects. For this study, the MMP was determined using correlations and calculations developed by Ahmadi and Johns (2011) and implemented as the output calculation in CMG's Winprop software package. While most methods use in-situ parameters such as GOR and

volume of cells, Ahmadi and Johns (2011) developed their output of MMP independent of such variables. More information on their method can be found in their publication. The values found for MMP in the output for HC Gas and CO_2 injection are 1880 psia and 2042 psia. These values are the minimum necessary pressures for miscibility in which the injection rates are determined. Equations are shown in the appendix.

6.2 Well Schedule Design

This section introduces the initial scenarios generated for miscible gas injection for the well completed in the Wolfcamp A-XY. The models use the same reservoir character and hydraulic fracturing model discussed in prior chapters, as well as producing via the base case scenario for several years prior to injection. The models also follow the huff-n-puff design already mentioned in this chapter.

The first scenario follows the HC gas injection method. Figure 33 presents the production profile of the well with cyclic injection starting in year 7, illustrating the primary production period along with the post injection cycle production period. Figure 35 shows the distribution of the injected gas in the most effected zone in the model. The production response can obviously be seen as moderately effective with just 3 cycles of HC gas injection. A moderate incremental recovery of 7.5% follows an optimistic outlook and can be attributed to an increase in flowing pressure, thus more flow, due to injection as well as the natural fracture network parameters. A reduction in average reservoir pressure compared to the base case can be seen in Figure 34, which is a result of the removal of a higher volume of hydrocarbons from the matrix and fracture network.

Even with the reduction in pressure, the contact of the fluids in the reservoir is continuing to be at above the MMP of 1880 psia, with a 500 mcf/d injection rate necessary to reach and maintain this pressure.

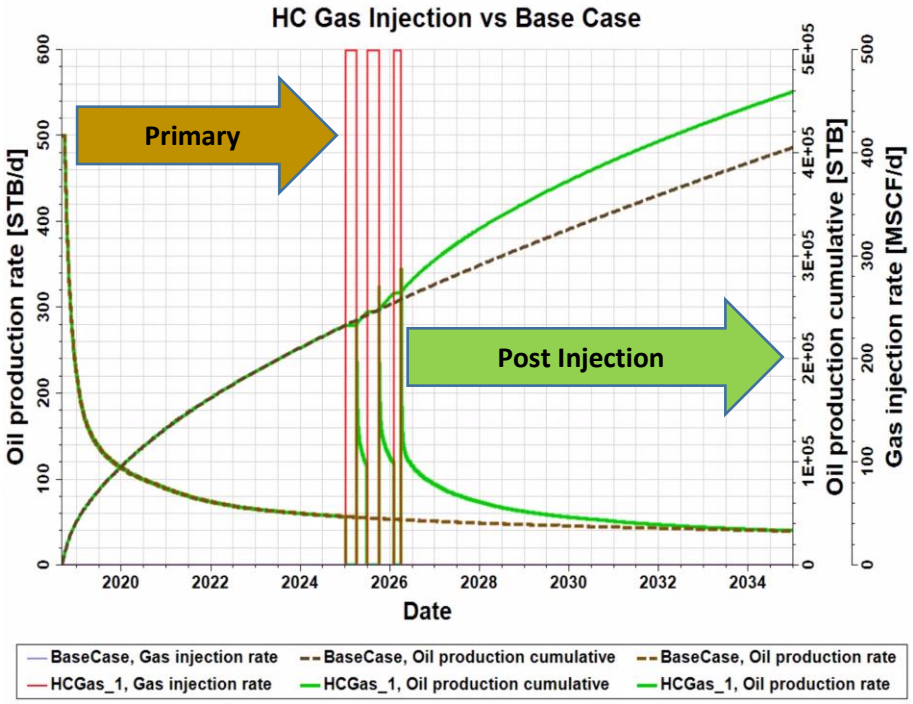

Figure 33. Production profile of HC gas injection during the primary and post injection phases.

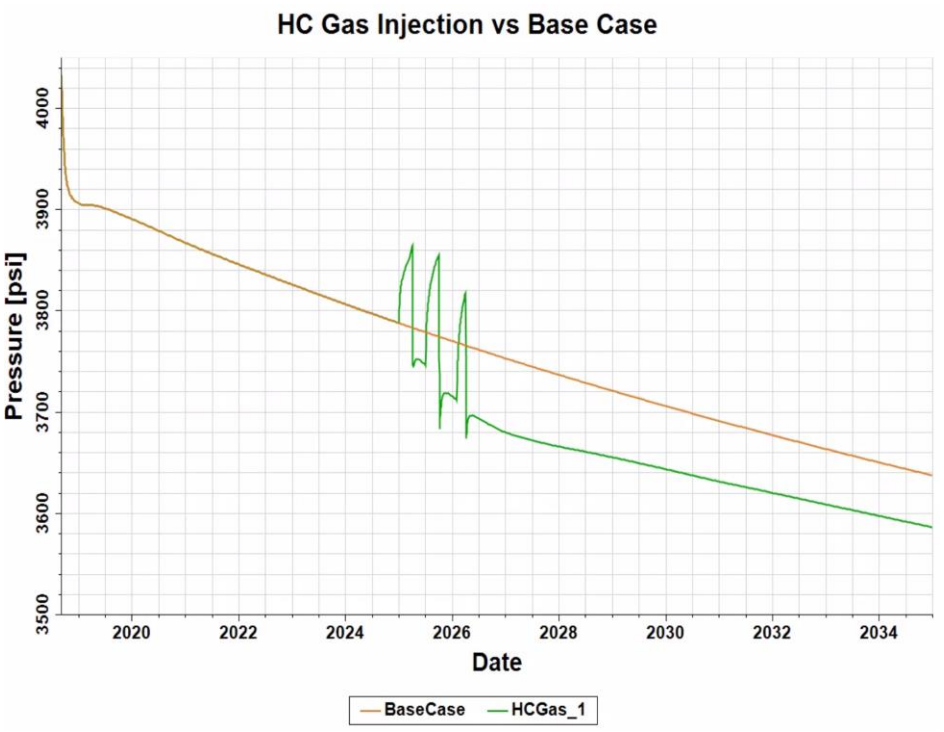

Figure 34. Average reservoir pressure during HC gas injection strategy.

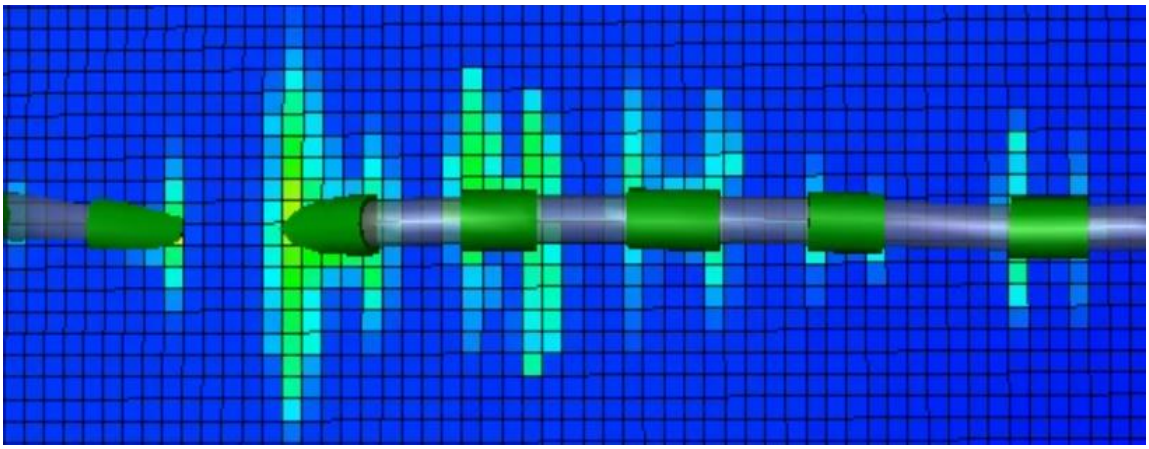

Figure 35. Distribution of HC gas injected into the formation and fractures.

A closer look into the results can be seen in Figure 36, showing the C7+ compositional tracking of the production profile. As one can see, when the HC gas is introduced into the injection stream and production returns, molar quantities of C7+ are removed at larger rates than compared to the base case. This result is consistent with the original production profile of the HC gas injection case.

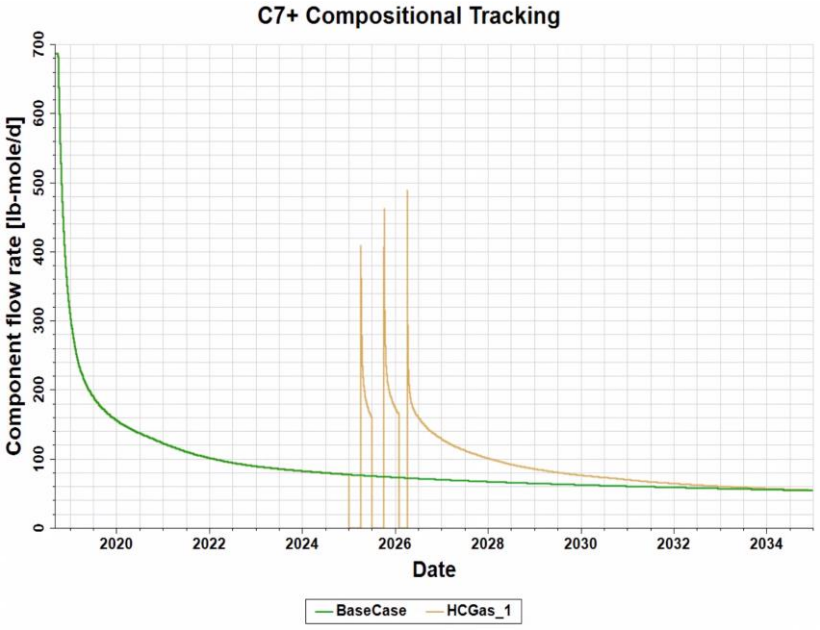

Figure 36. C7+ production tracking during HC gas injection strategy.

The second scenario depicts the injection of carbon dioxide (CO_2) as the EOR miscible method of recovery. The process follows the same injection timing, but an increased injection rate of 1000 mscf/day due to maintaining MMP pressure of at least 2042 psia. Figure 37 shows the production profile of the case with 3 cycles of injection followed by 3 months of production time. The result of the miscible injection is very similar to the HC gas case, however, significantly larger at approximately 9.5% incremental recovery. The distribution of CO_2 in the reservoir and natural

fracture system is illustrated in Figure 39, which shows to be contacting a larger volume of the reservoir than that of HC gas. Incremental pressure depletion also shows an increase, along with C7+ compositional tracking (Figure 38). However, an interesting feature of the compositional tracking profile is in reverse for the CO_2 injection model compared to the HC gas injection model.

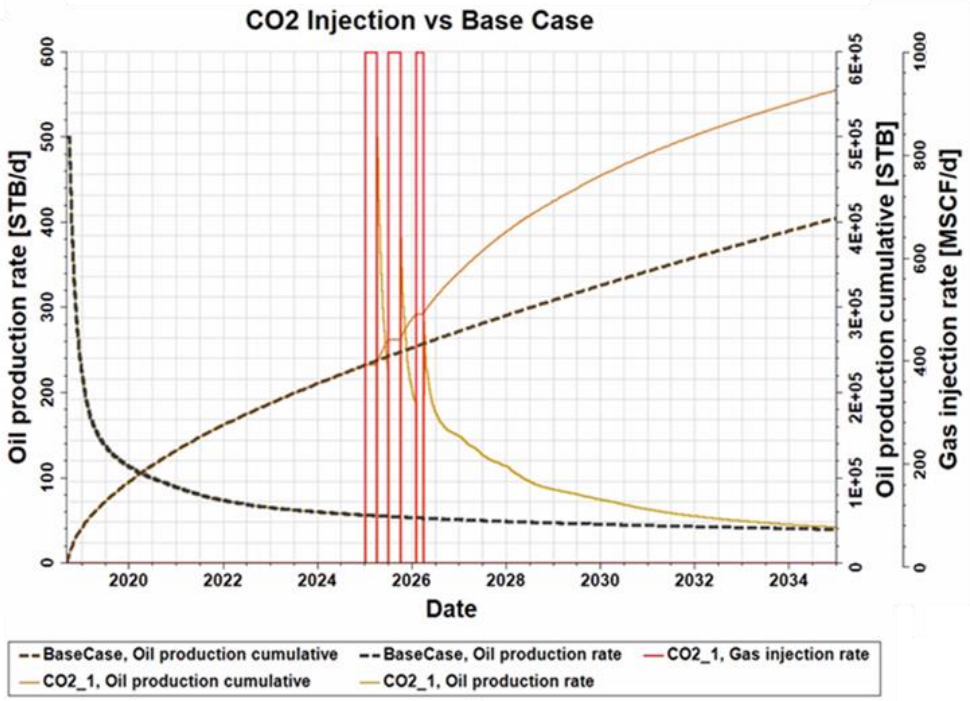

Figure 37. CO_2 injection production profile for 3 cycles of injection.

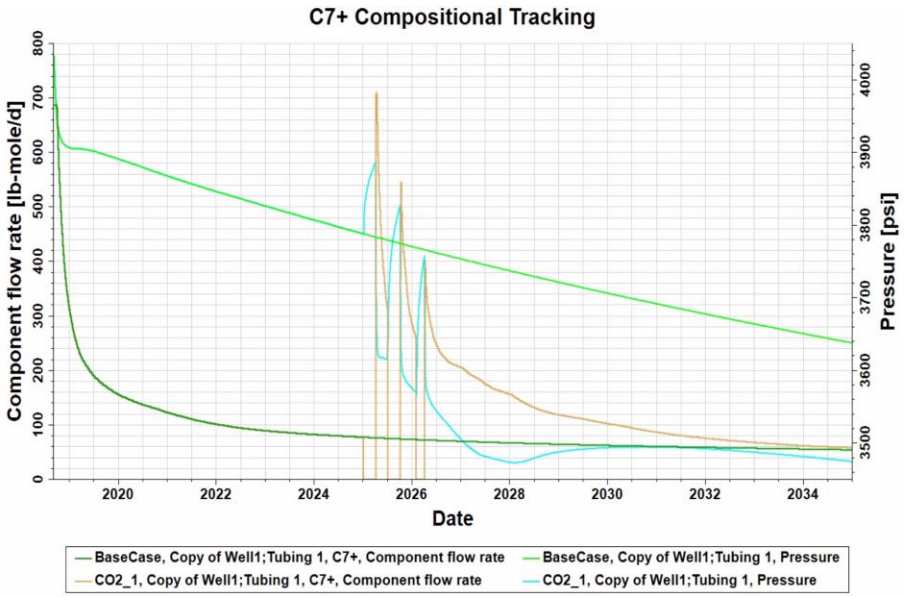

Figure 38. C7+ compositional production tracking for CO_2 injection strategy. Average reservoir pressure is also graphically shown.

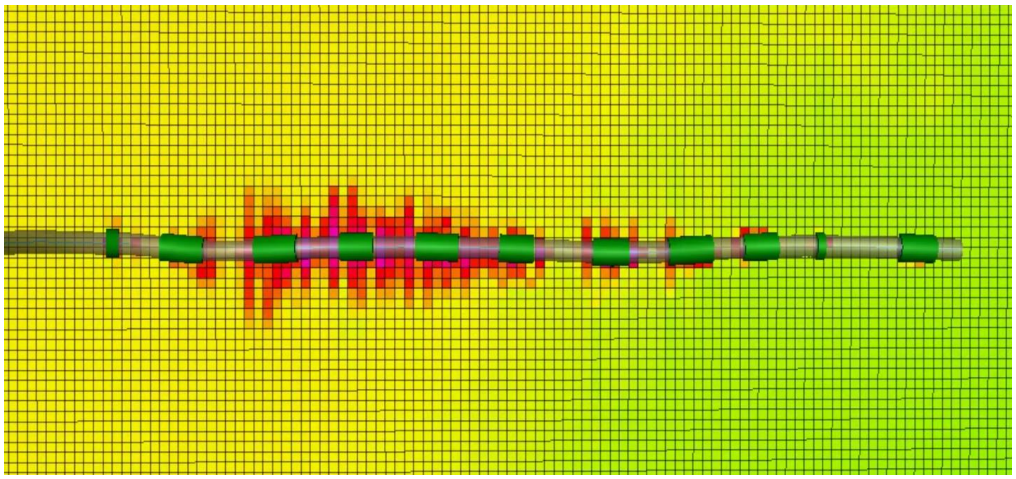

Figure 39. CO_2 distribution after injection in the 3D model.

6.3 Sensitivity Analysis

This section outlines three different sensitivities in the unconventional reservoir models, EOR miscible injection rates and timing of injection for each stream. Out of the 32 cases representing the dataset, the average case for each stream and base case was selected (Figure 40). Table 8 outlines the range of cases described in this study for the two injection streams. As discussed in the previous section, each type of miscible injection stream had different production profiles. The CO_2 injection case had the largest incremental recovery of 9.5%, while the HC gas case had a value of 7.5%. According to multiple studies, the driving mechanisms between the two injected gasses are molecular diffusion and injection rate (Mansour, Khalil, and Gamadi, 2017). With the values discussed for each in the prior sections, it is obvious that the difference in diffusion inputs for CO_2 and HC gas affects the resulting production profile. Accordingly, since less effective diffusion hinders production potential, it can also cause a lower injection rate capacity. As I noted in the previous section, CO_2 covers more of the reservoir than HC gas, contacting more rock and fluid volumes, thus creating more opportunity for diffusion and interfacial tension reduction with larger production rates (Figure 41, 42).

Table 8. Outcome of 16 cases for injection rate for each type of stream and the associated incremental recovery.

Injection Rate, mscf/d	Stream Type	Incremental Recovery, %
1000	HC Gas	3.2
1000	CO2	9.5
1250	HC Gas	2.7
1250	CO2	8.1
1500	HC Gas	2.3
1500	CO2	6.7
500	HC Gas	7.5
500	CO2	8.3
250	HC Gas	3.1
250	CO2	2.4
100	HC Gas	0.9
100	CO2	1.6
1750	HC Gas	-
1750	CO2	7.1
2000	HC Gas	-
2000	CO2	-

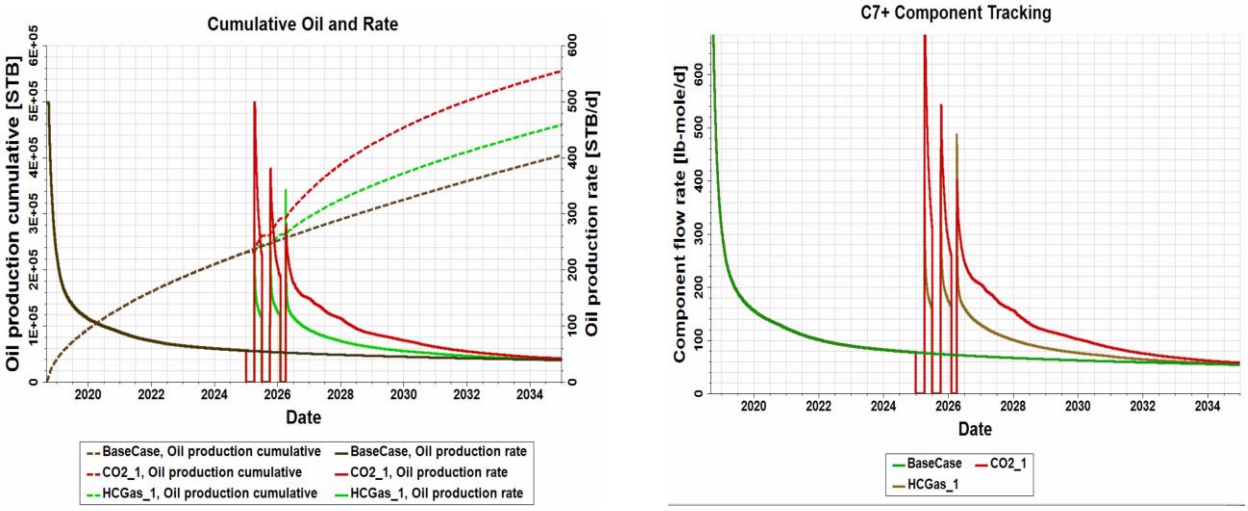

Figure 40. (A) Cumulative oil and rate comparison between HC gas, CO_2, and Base Case. (B) C7+ compositional production tracking for the 3 different cases.

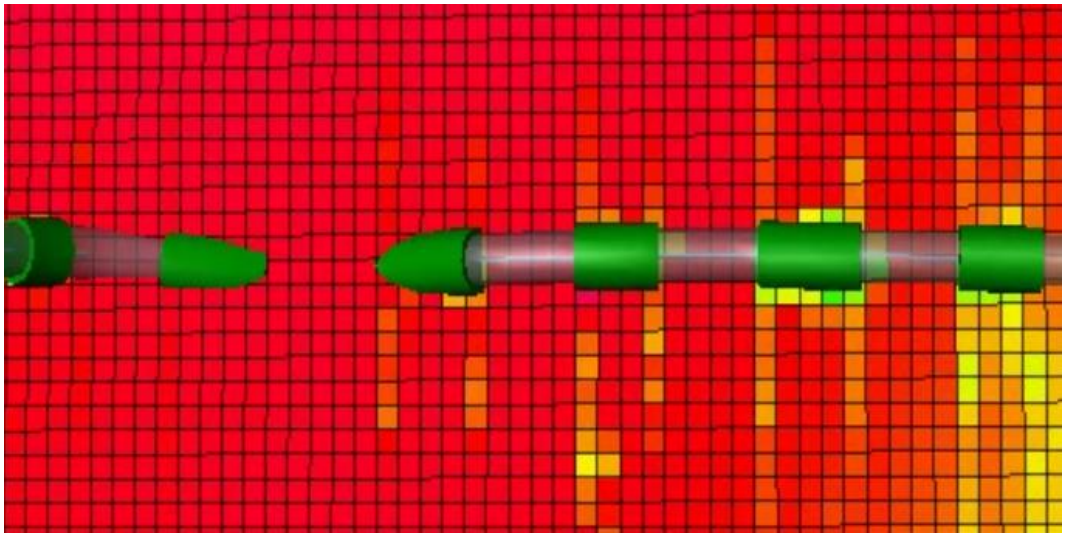

Figure 41. HC gas C7+ mole fraction remaining after 17 years.

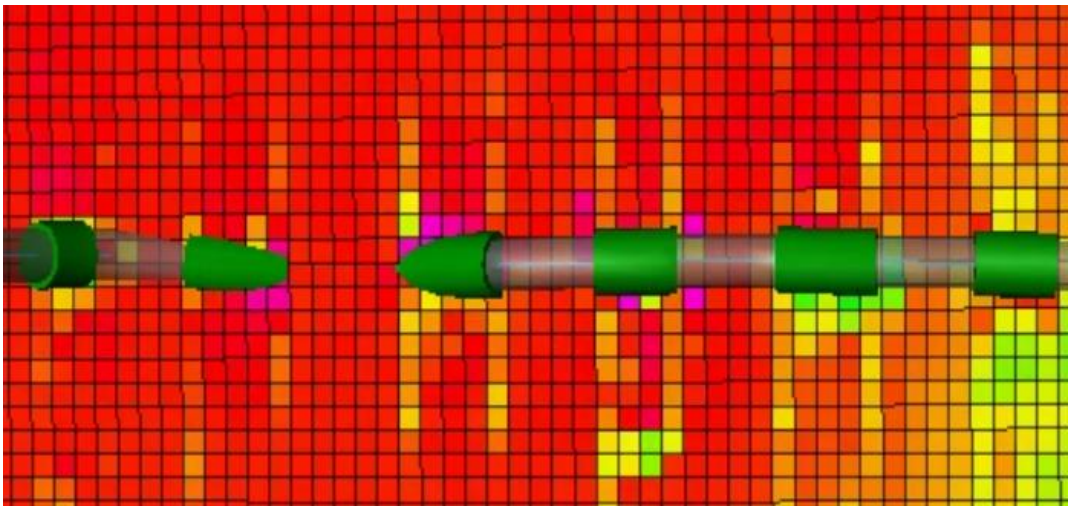

Figure 42. CO_2 injection C7+ mole fraction remaining after 17 years.

Additionally, this study presents sensitivity in timing of the start of injection for each EOR miscible stream. For these models, the injection rate of miscible gas is identical to the base case described in prior sections. Figures 43 and 44 give a graphical illustration of the minimum and maximum rates and incremental recovery found in 16 cases. All remaining cases fall in between each of the start times and do not show any clustering in the data. Due to simulator convergence and runtime issues, the range came out to be 2 to 9 years for the start dates of miscible injection. A significant outcome from this part of the study is that the incremental recovery is opposite for the observed time of injection between the HC gas and CO_2 streams (Figure 43). Additionally, HC gas injection has a smaller range of simulated outcomes (6.1-9.0%), while the CO_2 case has a range much larger (3.7-9.5%). For each case, Table shows the incremental increase and the time after initial production.

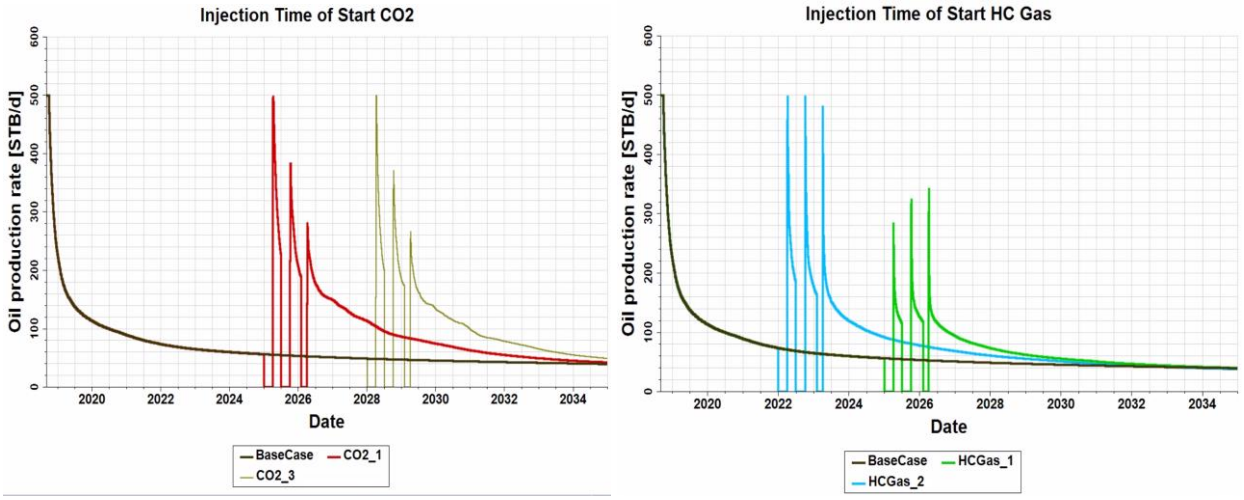

Figure 43. Time to injection production rate comparison between CO_2 injection and HC gas injection.

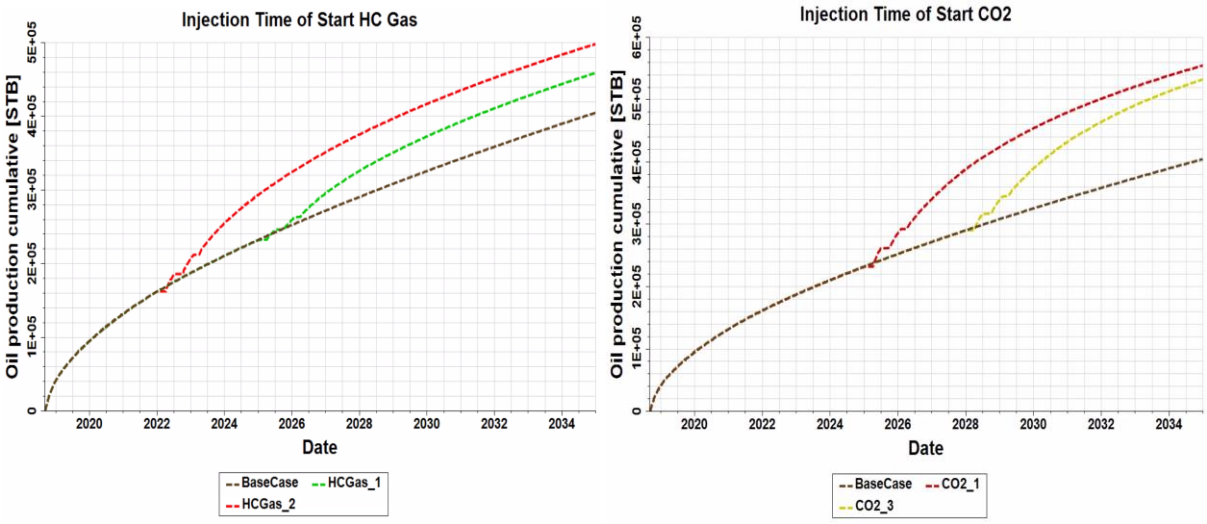

Figure 44. Time to injection cumulative production comparison between CO_2 injection and HC gas injection.

Table 9. Time to injection for each stream with incremental recovery results for 16 cases.

Time After Initial Production, years	Stream Type	Incremental Recovery, %
2	HC Gas	6.1
2	CO2	3.7
3	HC Gas	8.7
3	CO2	3.8
4	HC Gas	9.0
4	CO2	5.3
5	HC Gas	8.8
5	CO2	6.1
6	HC Gas	8.4
6	CO2	7.2
7	HC Gas	8.2
7	CO2	9.5
8	HC Gas	7.7
8	CO2	8.1
9	HC Gas	7.5
9	CO2	7.0

Chapter 7: Discussion and Limitations

The methodology discussed in Chapters 2 through 4 presented the core analysis, reservoir characterization and modeling of the well production scenario in the Wolfcamp A-XY. This process could simply be applied to any unconventional formation with the correct amount of data implemented. The 3D geological and mechanical earth model resulted in a reliable interpretation of the development area in question, while the hydraulic fracturing model data was incorporated from treatment pressures and real-time data. Laboratory and well log data reduced the uncertainty of the petrophysical and geomechanical properties amongst the variations in lithology. An importance to this study is that it comes from a currently producing well in the Delaware Basin with many future infill wells on a drilling schedule.

Although a significant amount of data was obtained for this study, dates of collection can give inaccuracies. When obtaining the core, the physical core is typically removed from the well at reservoir conditions and is moved to surface conditions, potentially altering properties when analyzing the core. This challenge can skew petrophysical and fluid inputs into the well model.

The study assumed that the development well was the only one in the area, ignoring the effect of wells completed in zones above and below the Wolfcamp A-XY. For more clarity, in offset areas of the basin, a no flow boundary does not exist between the zone above, Third Bone Spring sand, and the Wolfcamp A-XY, potentially effecting the production potential of the well. However, the objective of this study was to create a reliable, single well model that can be updated and used to predict future production performance in offset wells along with any efficiencies obtained with improved recovery.

The hydraulic fracturing workflow in GOHFER software in Chapter 4 depicted data that could be beneficial into understanding the geometry of the stimulated area around the well. The main constraint was implementing the geomechanical earth model from Chapter 3 to overlay the reservoir in the hydraulic fracturing software. Studying of important design inputs, such as process zone stress, aided in the understanding of implementing a range of parameters in a pressure history matching scenario.

Although a fluid sample was acquired prior to implementation into the model, the reservoir is assumed to have a homogeneous saturation of each component. This is a limitation of the model due to the fact that fluid could be a completely different compositional mixture within a few hundred feet away from the drained area. To mitigate this issue, more fluid samples could be taken in offset wells, including the producing well, prior to simulation.

Even though the 3D model is dual-porosity, transmissibility multipliers were used in the place of the hydraulic fracturing network. Implementing this data is quite simple and is only limited by the size of the grid blocks used in the model. To emphasize, the natural fracture network was incorporated as the second porosity, while the hydraulic fractures were imported as transmissibility multipliers normalized from fracture conductivity measurements in the output of the Gohfer model. The limitations to this method is that of pore space and pressure reduction. When a well is hydraulically fractured, pressure is increased in the stages. However, importing point data for pressure significantly reduces the capacity for the model to run and was removed from the study.

For an expanded study of this development area, a focus should be on the aforementioned limitations, along with a large data history match with measured production pressure and rates to reduce the uncertainty of reservoir characterization input values. Also, a greater understanding of

the miscible displacement process would be beneficial for prediction purposes. Due to time and computer capacity constraints, a larger data set of gas injection models could not be performed. An increase would decrease the uncertainty of the strategy.

Chapter 8: Conclusions

Implementing an integrated approach, this case study illustrates the importance of applying reservoir and hydraulic fracture modeling and simulation to develop unconventional formations in the Delaware Basin. The workflow consisted of using core data, fracturing treatment data, and fluid data obtained from the field to construct 3D geological and geomechanical models, hydraulic fracturing geometries, and reservoir fluid models consistent with the Wolfcamp A-XY formation. The study focused on the lifecycle of the well, utilizing primary and miscible EOR gas injection strategies. Changes in production with injection of both hydrocarbon gas (HC gas) and carbon dioxide (CO_2) show interesting trends with time to injection and gas type sensitivity. This case study concludes with the following takeaways:

- Transmissibility multipliers can partially be utilized to take the place of hydraulic fractures in a dual-porosity model using normalized fracture conductivity as the attribute. However, porosity and net pressure gained from the fracture is not a property for import ability, making this a limited approach.
- Core data combined with well log data and integrated into the 3D geological and mechanical model allow an accurate representation of the reservoir geometry and vertical variability in the Wolfcamp A-XY.
- Using the neural net correlation of well log data and lithology data in the model reduced uncertainty in the distribution of petrophysical and fluid properties in the reservoir model.

- The mineralogical profile coupled with core testing showed the variability of geomechanical properties throughout the reservoir. This was the main addition in simulating and matching hydraulic fracture stages in the software.
- For hydraulically fractured wells, modeling injection cycles of two different miscible gasses to reliably evaluate production performance is essential in enhancing the lifecycle of the well. Miscible injection of HC gas and CO_2 can add 2 to 9.5% in recovery within 17 years of the wells life.
- Time to injection results have the opposite effect between HC gas and CO_2 injection. HC gas has a higher incremental recovery in an earlier time to injection, while CO_2 has a significantly later time.
- There was shown to be a relationship between injection rate and incremental recovery for both miscible gasses. CO_2 has a larger necessary injection rate of 1000 mscf/d to reach its highest incremental recovery, while HC gas is much lower at 500 mscf/d.

Nomenclature

E	Young's Modulus, psia
x_f	Fracture half-length, ft
v	Poisson's Ratio, fraction
V_s	Shear Wave Velocity, ft/sec
V_p	Compressional Wave Velocity, ft/sec
WOC	Water-Oil Contact, ft (depth)
GOR	Gas-Oil Ratio, scf/bbl
w_f	Fracture Width, in
G	Bulk Modulus
K	Shear Modulus
T	Temperature, ^oF
P	Pressure, psia
V_{sh}	Shale Volume, %

References

Ahmadi, K., & Johns, R. T. (2011). Multiple-Mixing-Cell Method for MMP Calculations. *Society of Petroleum Engineers.*

Abouelresh, M. O., and Slatt, R. M. (2011). Shale Depositional Processes: Example from the Paleozoic Barnett Shale, Fort Worth Basin, Texas, USA. *Central European Journal of Geosciences*, 3(4), 398-409.

Barree and Associates LLC. (2017). GOHFER 3D User Manual. Obtained from barree.net/gohfer.

Barree, R. D. (2016). Fracture Conductivity and Cleanup in GOHFER. Obtained from gohfer.com.

Clavier, C., Coates, G., & Dumanoir, J. (1984). Theoretical and Experimental Bases for the Dual-Water Model for Interpretation of Shaly Sands. *Society of Petroleum Engineers.*

Cullick, A. S., Carrillo, M., Clayton, C., & Ceyhan, I. (2014). Well-spacing Study to Develop Stacked Tight Oil Pay in Midland Basin. *Society of Petroleum Engineers.*

Driskill, B., Pickering, J., & Rowe, H. (2018). Interpretation of High Resolution XRF Data from the Bone Spring and Upper Wolfcamp, Delaware Basin, USA. *Unconventional Resources Technology Conference.*

EIA, (2019). Permian Basin Wolfcamp and Bone Spring Shale Plays Geology Review. *U.S. Energy Information Administration.*

EIA, (2020). Short-Term Energy Outlook. *U.S. Energy Information Administration.*

Elhajjaji, R. R., Swedan, A., Behr, A., Awofodu, D. D., & Hincapie, R. (2017). Evaluation of a Chemical Enhanced Oil Recovery EOR Application in A Heterogeneous and Low Permeable Oil Reservoir: Advanced Screening by Reservoir Simulation. *Society of Petroleum Engineers.*

Ellis D.V., Singer J.M., (2007), Well Logging for Earth Scientists, *Springer*, Heidelberg, 692 p.

Haecker, A., Lakings, J., Marshall, E., & Ulla, J. (2017). A Novel Technique for Measuring (Not Calculating) Young's Modulus, Poisson's Ratio and Fractures Downhole: A Bakken Case Study. *Society of Petrophysicists and Well-Log Analysts.*

Hardie S. Nance and Harry Rowe, (2015), Eustatic Controls on Stratigraphy, Chemostratigraphy, and Water Mass Evolution Preserved in a Lower Permian Mudrock Succession, Delaware Basin, West Texas, USA, Interpretation 3.

Hawthorne, S. B., Miller, D. J., Grabanski, C. B., Sorensen, J. A., Pekot, L. J., Kurz, B. A., … Melzer, S. (2017). Measured Crude Oil MMPs with Pure and Mixed CO_2, Methane, and Ethane, and Their Relevance to Enhanced Oil Recovery from Middle Bakken and Bakken Shales. *Society of Petroleum Engineers.*

Holanda, R. W. de, Gildin, E., & Valko, P. P. (2018). Combining Physics, Statistics, and Heuristics in the Decline-Curve Analysis of Large Data Sets in Unconventional Reservoirs. *Society of Petroleum Engineers.*

Kilgore, E. C., Land, A. G., Schmidt, A. W., & Yunker, J. D. (1972). Applications of the Coriband Technique to Complex Lithologies. *Society of Petrophysicists and Well-Log Analysts.*

Kovscek, A. R. (2002), Screeening Criteria for CO_2 Storage in Oil Reservoirs. *Pet. Sci. Technol.* 2002, 20, 841-866.

Kurtoglu, B., & Kazemi, H. (2012). Evaluation of Bakken Performance Using Coreflooding, Well Testing, and Reservoir Simulation. *Society of Petroleum Engineers.*

Kvale, E. P., & Rahman, M. (2016). Depositional Facies and Organic Content of Upper Wolfcamp Formation (Permian) Delaware Basin and Implications for Sequence Stratigraphy and Hydrocarbon Source. *Unconventional Resources Technology Conference.*

Malik, M., Schmidt, C., Stockhausen, E. J., Vrubel, N. K., & Schwartz, K. (2013). Integrated Petrophysical Evaluation of Unconventional Reservoirs in the Delaware Basin. *Society of Petroleum Engineers.*

Mansour, A. G., Khalil, R., & Gamadi, T. (2017). Compositional Simulation Evaluation of Miscible Gas Injection Performance in Tight Oil Formation. *Society of Petroleum Engineers.*

Ojha, S. P., Misra, S., Sinha, A., Dang, S., Tinni, A., Sondergeld, C., Rai, C., (2017). SPE-187398-MS Relative Permeability and Residual Saturation Estimates for Organic-Rich Shale Samples from the Bakken, Wolfcamp, Eagle Ford and Woodford Formations.

Phan, T. N., Cronk, B. R., Almasoodi, M. M., & Reza, Z. A. (2018). Lithologic and Geomechanical Control on CO_2 Huff-n-Puff Enhanced Oil Recovery Processes Using Integrated Modeling Framework in Wolfcamp. *Unconventional Resources Technology Conference.*

Rittenhouse, S., Li, Y., Hughston-Kennedy, K., Fritz, J., Pritchard, J., Cassel, L., … Mooney, T. (2017). Delaware Basin Leonard Reservoir Characterization, New Mexico and Texas. *Unconventional Resources Technology Conference.*

Salman, M., Kostarelos, K., Sharma, P., & Lee, J. H. (2019). Application of Miscible Ethane Foam for Gas EOR Conformance in Low-Permeability Heterogeneous Harsh Environments. *Unconventional Resources Technology Conference.*

Schlumberger (2018) https://www.software.slb.com/products/petrel. Accessed 12 September, 2019.

Schlumberger (2019) https://www.software.slb.com/products/techlog. Accessed 5 August, 2019.

Spaid, J. S., Dahl, J. A., Dusterhoft, R., McDaniel, B. (2016). Shale Reservoir Centric-Completions. *The Open Petroleum Engineering Journal 9* (Suppl-1,M6): 92-106.

Taylor, T., Waters, G. A., Sturm, S., Singh, M., Hamilton, D., Le Calvez, J. H., & Miller, C. K. (2013). Evaluating the Impact of Mineralogy, Natural Fractures and In Situ Stresses on Hydraulically Induced Fracture System Geometry in Horizontal Shale Wells. *Society of Petroleum Engineers.*

Victorino, I. R. S., Filho, J. C. H., Castro, M. S., Schiozer, D. J. (2016). Sensitivity Analysis of Production System Parameters for Integrated Simulation of Reservoir-Production Systems. Rio Oil & Gas Expo and Conference, Rio de Janeiro, Brazil.

Zhang, Y., Mostaghimi, P., Fogdon, A., Arena, A., Sheppard, A., Middleton, J., & Armstrong, R. T. (2017). Determination of Local Diffusion Coefficients and Directional Anisotropy in Shale from Dynamic Micro-CT Imaging. *Unconventional Resources Technology Conference.*